Experimental searches for the neutron electric dipole moment

2009 J. Phys. G: Nucl. Part. Phys. 36 104002

(http://iopscience.iop.org/0954-3899/36/10/104002)

J. Phys. G: Nucl. Part. Phys. **36** (2009) 104002 (37pp) doi:10.1088/0954-3899/36/10/104002

Experimental searches for the neutron electric dipole moment

S K Lamoreaux[1] **and R Golub**[2]

[1] Department of Physics, Yale University, USA
[2] Department of Physics, North Carolina State University, USA

E-mail: steve.lamoreaux@yale.edu and rgolub@ncsu.edu

Received 22 June 2009
Published 16 September 2009
Online at stacks.iop.org/JPhysG/36/104002

Abstract
The possible existence of a neutron electric dipole (EDM) was put forward as an experimental question in 1949, 60 years ago, and still remains an outstanding question in modern physics. A review of the technical innovations that allowed for improving the experimental limit by nearly eight orders of magnitude (approximately a decade per decade) will be presented, along with a discussion of the prospects for further improvement.

1. Introduction: a prehistory of symmetry in modern particle physics

Evidence that forces more complicated than the Coulomb interaction are necessary to describe the subatomic world came with the discovery of the deuteron quadrupole moment by Kellog, Rabi, Zacharias and Ramsey in 1939 [1], indicating that the nuclear forces binding the deuteron together have a tensor character. This idea was carried forward, as an experimental question, by Ramsey and Purcell [2] who together asked whether the nuclear force 'conserves' parity. At this time, it was also well known that the neutron, although electrically neutral, possesses a magnetic moment hence is a composite particle. If the charged internal constituents of the neutron are displaced from the center of mass, for example, the neutron can have an electric dipole moment (EDM) given by

$$\vec{d} = \int \mathrm{d}^3x \langle \psi | \Sigma_i q_i \vec{r}_i | \psi \rangle \equiv e d_n \vec{\sigma}, \tag{1}$$

where i labels the charge constituents of the neutron and e is the absolute value of the electron charge. This is zero if $|\psi\rangle$, the neutron ground state wavefunction is a state of definite parity. The EDM like any vector must lie along the neutron spin. In addition, the neutron ground state must be (as it is known to be from neutron scattering or molecular spectra) non-degenerate in order for the observation of a non-zero neutron EDM to be evidence of P and/or T non-conservation.

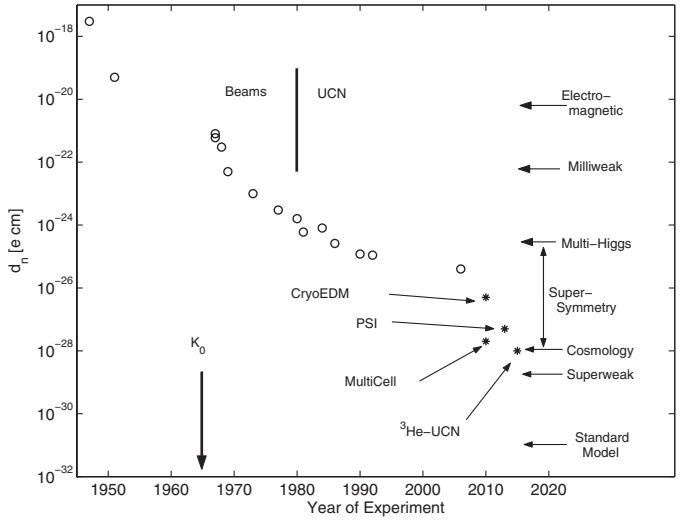

Figure 1. History of the sensitivity of neutron EDM searches, compared with some theoretical suggestions as to the magnitude. The use of stored ultracold neutrons (UCN) eliminated the motional magnetic field effect that was a limiting systematic for neutron beam experiments, as described in the text. The points marked with * are the anticipated limits from experiments presently under development or proposed, and will be discussed in this paper.

Emboldened by these ideas, Smith, Purcell and Ramsey performed an experimental test of this hypothesis with a neutron beam magnetic resonance where a shift in the neutron Larmor frequency was sought when an electric field, in addition to a magnetic field, was applied,

$$\omega_{\pm} = \gamma B_0 \pm 2ed_n E/\hbar, \tag{2}$$

where $\pm$ refers to the relative orientation of the applied magnetic B_0 and electric E fields (parallel or antiparallel), the factor of 2 comes from the energy difference between the two spin states, and $\hbar$ (Planck's constant) converts the energy $ed_n E$ to a frequency. d_n is almost always specified in the units e cm, where e is the absolute value of the electron charge.

This first experimental test, performed at Oak Ridge in 1950 however not reported until 1957 [3], produced a null result, but became of interest when the question of parity violation in weak interactions was brought to the forefront of physics in the mid-to-late 1950s. At the time of the original suggestion of parity violation in the weak interactions [4], the (unpublished) 1950 result for the neutron EDM was the best existing limit on parity violation. Parity symmetry violation was discovered in beta decay shortly afterward [5], and it was pointed out by Landau that the existence of a non-zero EDM of an elementary particle would also violate T and CP conservation, because, as was well known, the results of any combined operations of C (charge conjugation) together with P and T (time reversal) must satisfy $CPT = 1$ for fundamental interactions to preserve Lorentz invariance. Ramsey argued that the question of the existence of a neutron EDM was therefore still open [6], although this possibility was not taken too seriously until a CP non-invariant process, implying a time-reversal T non-invariance, was observed in the decay of the neutral K_0 particle.

This discovery, made in 1964, brought the neutron EDM question to the forefront of fundamental physics, where it remains. Shown in figure 1 is a history of neutron EDM limits together with some theoretical model predictions that have been tested, or remain to be tested

or otherwise constrained. There are several features of the neutron EDM search, implicit in this figure, that deserve comment:

(i) The Standard Model of Electroweak interactions, which described the *CP* violation observed in K_0 decay by a single complex parameter, predicts a neutron EDM less than 10^{-32} e cm, which is impossibly small to measure by any currently known technology. The electron EDM in the Standard Model is predicted to be even smaller, 10^{-40} e cm. However these estimates neglect the so-called θ problem, the existence of a large *CP* violating term in the standard model Lagrangian that predicts a very large EDM. Attempts to reconcile this with the smallness of current EDM estimates have led to the axion hypothesis and have spawned an industry of experiments (so far unsuccessful) to search for such a particle.

(ii) Since the Standard Model prediction is so small, the neutron and other EDMs are particularly sensitive to new physical processes, such as *CP* non-invariance in supersymmetry. The precision measurements of the *CP* properties of 'strange' particles (e.g., strange K and B mesons) require precision perturbative QCD calculations to ascertain new physical processes beyond the allowed Standard Model processes, and are thus severely hampered in the discovery of new *CP* violation effects below a few per cent of the usual Standard Model effect.

(iii) The baryon–antibaryon asymmetry observed in the Universe requires *CP* non-invariance at a greater level than given by the Standard Model. A minimum neutron EDM calculated from proposed interactions that produce the observed asymmetry, and that are compatible with strange particle properties, suggests a neutron EDM near 10^{-28} e cm.

Thus, we expect that the neutron and other EDM searches will remain essential for the understanding of *CP* and *T* non-invariance in fundamental processes. For example, given the apparent and anticipated difficulties of even observing the Higgs boson at the Large Hadron Collider, it appears as unlikely that the specific symmetry properties of the Higgs will be measured, at least not for the foreseeable future. At present, the best EDM limit for any particle or system is that of the ^{199}Hg atom, which is $d_{\rm Hg} < 3.1 \times 10^{-29}$ e cm [7]. This corresponds to a neutron EDM of order 5.8×10^{-26} e cm because of the intrinsic loss of sensitivity due to the electron cloud which surrounds the Hg nucleus and shields the externally applied electric field at the nucleus. The present goal for neutron EDM searches is to push the sensitivity a level below 10^{-27} e cm, while attainment of a sensitivity below 10^{-28} e cm would allow testing models of the baryon asymmetry of the Universe.

Readers whose thirst for knowledge is not quenched by this paper can find further details in [8] and [9].

2. Properties of the neutron

As all direct neutron EDM searches involve the use of free neutrons, a brief review of the properties of the neutron and its interactions with matter and fields is warranted.

Neutrons account for about half of all the masses around us; yet, the neutron was only discovered in 1932, the same year that the positron was discovered, and the year in which deuterium was isolated for the first time. This late discovery as compared to the electron and proton is due in part to the fact that the free neutron is unstable with respect to β decay, with a lifetime now known to be 885 ± 0.2 s, with the most accurate values obtained from ultracold neutron storage experiments. In fact, the existence of the neutron was postulated as early as 1923 to explain the possible existence of isotopes. Originally, the neutron tended to be thought of as a super-bound hydrogen atom (although a new interaction in addition to the Coulomb

Table 1. Currently accepted properties of the neutron.

Property	Value
Intrinsic spin I	$1/2$
Mass m_n	$939.565\,63 \pm 0.000\,28$ MeV
Mean life τ	$885.7 \pm .2$ s
Magnetic moment μ	$-1.913\,0427 \pm 0.000\,0005\ \mu_N$
Electric dipole moment d	$<0.29 \times 10^{-25}\ e$ cm (95% conf)[a]
Electric polarizability α	$(11.6 \pm 1.5) \times 10^{-4}$ fm^3
Charge q	$(-0.4 \pm 1.1) \times 10^{-21}\ e$

[a] The value as presented here will be discussed in section 6.

force would be required for this); the neutron mass as first measured indicated that indeed this model might be correct. Subsequently, it was realized that the gamma energy associated with the photodisintegration of the deuteron allows a very precise neutron mass measurement, and the result indicated that the neutron was probably unstable with respect to β decay [10]. Neutron β decay was first directly observed in 1948 [11].

Measurements of the deuteron magnetic moment, most notably by Rabi and associates, were the first indications that the neutron itself has an intrinsic magnetic moment; in these experiments, it became evident that the deuteron has a quadrupole moment, as mentioned earlier. The results obtained by Rabi *et al* could not uniquely determine the magnitude of the neutron magnetic moment nor its sign; the first quite definite indication of the neutron spin and magnetic moment magnitude was found by Fermi [12]. It was shown that the observed rate of capture of neutrons by hydrogen (protons) could well be described by a spin–spin interaction assuming that both the neutron and proton have spin $1/2$, and this can be considered the first firm proof that the neutron is a spin-$1/2$ system. This was subsequently directly shown through neutron beam magnetic resonance experiments; the neutron magnetic moment is now known to a few parts in 10^7. Table 1 lists the currently accepted properties of the neutron, as given by the particle data group [13].

3. Interaction of neutrons with matter

The interaction between a neutron and a proton can be represented (when the relative velocity is sufficiently small) by an attractive spherical square-well potential with a depth U_0 of about 40 MeV and a radius R of about 2 fermi (1 fermi $= 10^{-15}$ m). The force between a neutron and a heavier nucleus has essentially the same form, with the well depth remaining nearly constant, and radius growing approximately as $r_0 A^{1/3}$, where A is the total number of nucleons (constant nuclear density). For our present discussion, we can assume that there is no neutron–electron interaction.

Slow neutrons, by definition, have a de Broglie wavelength $\lambda = 2\pi\hbar/mv$ (m is the neutron mass, v is the neutron velocity) which satisfies

$$\frac{2\pi R}{\lambda} = kR \ll 1. \tag{3}$$

In the region where $r > R$, i.e., where the neutron–nucleus potential $U(r) = 0$, we can write the total neutron wavefunction (incident plane wave plus scattered wave) as

$$\psi = \mathrm{e}^{\mathrm{i}\vec{k}\cdot\vec{r}} + f(\theta)\frac{\mathrm{e}^{\mathrm{i}kr}}{r}. \tag{4}$$

When equation (3) is satisfied, the scattering is predominately s wave, and we can write

$$f(\theta) = \text{constant} = b = -a, \tag{5}$$

where a is called the coherent scattering length, and b the scattering amplitude. The differential scattering cross-section is

$$\frac{\mathrm{d}\sigma}{\mathrm{d}\Omega} = |f(\theta)|^2 \tag{6}$$

which in the case of s wave scattering is constant.

In the range $R < r < 1/k$, equation (4) can be written in the form

$$\psi \approx 1 - a/r = (r - a)/r. \tag{7}$$

Since $\psi = 0$ at $r = a$, a can be interpreted as the radius of a hard sphere which would produce the same scattered wavefunction at $r \gg a$ as does the actual potential. When the sign of a is defined as in equation (5), as was done originally in [14], $a > 0$ indicates that the wavefunction is pushed away from the origin, and one would conclude, on looking at the scattered wavefunction at great distances from the origin, that the neutron–nucleus interaction is repulsive.

If we transform the scattered wavefunction into $u = r\psi$, in the region $r < R$, u has the form

$$u = A \sin Kr, \qquad K = \sqrt{k^2 + \frac{2mU_0}{\hbar^2}}, \tag{8}$$

which must satisfy the boundary conditions $u = 0$ at $r = 0$ (guaranteed) and that u'/u be continuous at $r = R$. From equations (7) and (8),

$$a/R = 1 - \frac{\tan KR}{KR}. \tag{9}$$

Only when $\tan KR > KR$ it is possible that $a < 0$; thus, except for $KR < \pi/2$, the likelihood that $a < 0$ is very small. It turns out that $KR > 3$ for all nuclei, with the exception of hydrogen, so nuclei with negative scattering lengths are expected to be rare [15]. This is observed experimentally, with $a < 0$ for hydrogen and only three or four other known isotopes. Since the strong interaction is spin dependent, a can also be spin dependent (see [16], section 132).

In addition to being scattered, neutrons can also be captured (absorbed) by nuclei, which can lead to the emission of a γ ray or charged particles. The probability for such reactions is proportional to $|M|^2/(\text{incident flux})$ where

$$M = \langle \psi_\mathrm{f} | V | \psi_\mathrm{i} \rangle. \tag{10}$$

Here $\psi_{\mathrm{f,i}}$ refer to the incident and final neutron/nucleus compound states, and V is the neutron–nucleus interaction. By arguments similar to those showing that $f(\theta)$ is independent of incident neutron energy, it can be shown that M is also. Thus, the absorption probability is proportional to

$$1/(\text{incident flux}) = 1/v.$$

A neutron beam of intensity I_0 will be attenuated on propagation through matter by

$$I(L) = I_0\, \mathrm{e}^{-\rho\sigma L}, \tag{11}$$

where ρ is the number of nuclei per unit volume, σ is the total cross-section (scattering plus absorption) with the inelastic (neutron energy changes) and absorption cross-section usually

being proportional to $1/v$, and L is the distance into the target that the neutron beam has propagated. It is also possible to think of absorption as simply a rate of neutron loss while in the presence of matter:

$$\sigma L = \sigma_0 \frac{v_0}{v} L = \sigma_0 v_0 t, \tag{12}$$

where σ_0 is the absorption cross-section measured at v_0, and $t = L/v$. Note that no assumptions have been made about the velocity of the absorbers; in fact, even for neutron absorption by a gas, the relevant velocity is that of the neutrons relative to the center of mass of the absorbers. The relevant parameter is the time that the neutron spends in the vicinity of the absorbers. (This is true only in the absence of very low energy resonances.)

To describe the interaction of slow neutrons with bulk matter or molecules, Fermi developed the concepts of the effective or 'pseudo' potential and the neutron index of refraction [14] (see also [16], section 151). His idea is as follows. Although the range of nuclear forces is small, they are quite strong within that range so one cannot in general apply perturbation theory to a collision between a neutron and a nucleus. However, as we have shown, the scattering amplitude for slow neutrons is a constant independent of incident neutron velocity. The constant amplitude can be reproduced if we describe the neutron–nucleus interaction as a point interaction

$$U(\vec{r}) = -\frac{2\pi\hbar^2}{M} b\delta(\vec{r}), \tag{13}$$

where M is the neutron–nucleus reduced mass and b is the constant scattering amplitude. When this potential is substituted into the Born approximation,

$$b = -\frac{M}{2\pi\hbar^2} \int U(\vec{r})\, \mathrm{e}^{-\mathrm{i}\vec{q}\cdot\vec{r}}\, \mathrm{d}V, \tag{14}$$

the δ function makes the integral independent of momentum transfer $\vec{q}$.

When many scatterers are bound in a piece of bulk matter, the potential seen by a neutron is, recalling $b = -a$,

$$U_F(\vec{r}) = \frac{2\pi\hbar^2}{m} \sum_i a_i \delta(\vec{r} - \vec{r}_i), \tag{15}$$

where $m \approx M$, and i labels a particular nucleus bound in the material. Thus, a neutron incident on a piece of matter (solid, liquid or gas) will see a 'forest' of δ-function potentials. The neutron wavefunction will then consist of the incident wave and a sum of the spherical waves scattered by each nucleus,

$$\psi(\vec{r}) = \mathrm{e}^{\mathrm{i}\vec{k}\cdot r} - \sum_i a_i \frac{\mathrm{e}^{\mathrm{i}k|r-r_i|}}{|r - r_i|} \psi(\vec{r}). \tag{16}$$

This equation serves as the starting point for multiple scattering calculations. With $\psi(\vec{r})$ on the rhs replaced by $\mathrm{e}^{\mathrm{i}\vec{k}\cdot r_i}$ it is the usual starting point (Born approximation) for calculation of the effects of bulk material on the neutron wavefunction (see [17] or [18] for a more complete treatment, and [19] for a discussion of appropriate approximations). The effects in the long wavelength limit can be understood more simply by consideration of a neutron wave packet inside an extended material body:

$$\psi(\vec{r}) = \int g(\vec{k})\, \mathrm{e}^{-\mathrm{i}\vec{k}\cdot\vec{r}}\, \mathrm{d}^3k. \tag{17}$$

In the very long wavelength limit, there is no diffraction, and to first order, the effect of the material on the neutron total energy is

$$\begin{aligned}\delta E &= \langle\psi|U_F|\psi\rangle \\ &= \frac{2\pi\hbar^2}{m}\iiint \mathrm{e}^{\mathrm{i}\vec{k}\cdot\vec{r}}\,\mathrm{e}^{-\mathrm{i}\vec{k}'\cdot\vec{r}}\,g^*(\vec{k})g(\vec{k}')\sum_i a_i\delta(\vec{r}-\vec{r}_i)\,\mathrm{d}^3r\,\mathrm{d}^3k\,\mathrm{d}^3k'. \end{aligned} \tag{18}$$

We are interested in the long wavelength limit, and elastic scattering: $|k| = |k'|$, so

$$\delta E = \frac{2\pi\hbar^2}{m}\int |\psi(\vec{r})|^2\sum_i a_i\delta(\vec{r}-\vec{r}_i)\,\mathrm{d}^3r. \tag{19}$$

We can choose the neutron wavefunction to be of arbitrary shape; assume that it is constant through a small spherical volume V. Then the first-order energy becomes

$$\delta E = \frac{2\pi\hbar^2}{m}\sum[\rho a]_k/V = \frac{2\pi\hbar^2}{m}\langle\rho a\rangle_V, \tag{20}$$

where $[\rho a]_k$ is the number density and scattering length for a particular isotope, and $\langle\rangle_V$ represents an average over V of the scattering lengths and densities of the different isotopes within the small volume. If we consider a neutron with total energy $E = \hbar^2k_0^2/2m$ outside the material, inside the total energy is the same, so

$$k_0^2 = k^2 + 4\pi\langle\rho a\rangle_V. \tag{21}$$

Because k changes on entering the material, we can define a material index of refraction, as a function of position in an inhomogeneous material,

$$n(\vec{r}) = \sqrt{1-\frac{4\pi[\rho a(\vec{r})]}{k_0^2}}, \tag{22}$$

or an effective potential

$$U(\vec{r}) = \frac{2\pi\hbar^2}{m}[\rho a(\vec{r})]. \tag{23}$$

For a pure homogeneous material,

$$U_{\mathrm{F}} = \frac{2\pi\hbar^2}{m}\rho a. \tag{24}$$

Thus, the surface of a piece of bulk matter represents a potential step of height U_{F} to an entering neutron. Most interestingly, this potential is *repulsive* for the vast majority of nuclei ($a > 0$) even though the neutron–nucleus potential is attractive. This is because the effective potential is the volume average of the Fermi potential, which is repulsive for an attractive neutron–nucleus potential; this is a consequence of matching the boundary conditions at the nucleus surface. Because the potential U_{F} is independent of neutron energy while the neutron index depends on the neutron energy, for many applications, the potential is the more useful quantity.

Absorption can be modeled as an imaginary potential; we saw before that the rate of neutron absorption within a material is given by $\rho\sigma_0 = \Gamma$. If we write

$$\psi(t,\vec{r}) = \mathrm{e}^{(-\mathrm{i}\omega-\Gamma/2)t}\psi(\vec{r}), \tag{25}$$

where ω represents the total energy, we see that the neutron probability decreases as $\mathrm{e}^{-\Gamma t}$. Since the neutron wavefunction, if it is an eigenstate, evolves as $\mathrm{e}^{-\mathrm{i}\Lambda t}$ where Λ is the eigenvalue, it is apparent that

$$\Lambda = \frac{\hbar^2}{2m}k_0^2 + U_{\mathrm{F}} + \mathrm{i}\Gamma/2 \tag{26}$$

Table 2. Neutron optical properties of selected materials.

Element	ρ (10^{22} cm^{-3})	$\langle a_{\rm coh}^{\rm bound}\rangle$ (fm)	$U_{\rm F}$ (neV)	$v_{\rm crit}$ (m s^{-1})	σ_0(18 Å) (barn)	$f = W/U_{\rm F}$ ($\times 10^{-5}$)
^{58}Ni	9.0	14.4	335	8.0	44	8.6
C (diamond)	17.6	6.6	303	7.6	–	–
BeO	7.25	13.6	261	7.1	6.6	1.35
Ni	9.0	10.6	252	7.0	48	12.5
Be (300 K)	12.3	7.75	252	7.0	1.4	0.5
^{65}Cu	8.93	11.0	224	6.6	28	7.0
Fe	8.5	9.7	210	6.3	30	8.5
C (graphite)	10.0	6.6	180	5.9	30	8.5
D-plexiglas $(C_2D_3O)_n$	1.65	39.11	168	5.7	–	–
D-polystyrene $(CD)_n$	4.76	13.3	165	5.6	–	–
Teflon $(CF_2)_n$	2.65	17.6	123	4.9	–	–
Pb	3.29	9.6	83	3.	2.0	0.6
Al	6.02	3.45	54	2.0	2.8	2.25
Plexiglas $(C_2H_3O)_n$	1.65	7.88	33.9	2.6	1.0	
V	7.1	−0.382	−7.2	–	50	–
Polyethylene $(CH_2)_n$	3.9	−0.84	−8.7	–	–	
H_2O	3.34	−1.68	−14.7	–	–	
Ti	5.6	−3.34	−48	–	58	–

for a neutron with wave number k_0 outside the material. This motivates us to write the Hamiltonian as

$$H = p^2/2m + U_{\rm F} - {\rm i}W, \tag{27}$$

where $W = \hbar\rho\sigma_0 v_0/2$.

This Hamiltonian forms the basis of the field of neutron optics (see, for example, [17]) and represents the one-dimensional potential step well known from all introductory texts on quantum mechanics, except here we have allowed for a complex potential to describe the absorption of neutrons.

If a neutron is incident obliquely on a material surface at an angle θ relative to the surface normal, we can transform it into a frame where the component of the velocity parallel to the surface is zero; if the kinetic energy given by the perpendicular component of the velocity is less than $U_{\rm F}$ for the material, the neutron will be totally reflected from the surface. Table 2 lists the properties and effective potential of some elements and common materials.

This reflection can also be understood from an optical point of view. The refraction of neutrons at material surfaces is exactly analogous to that of light waves (for the electric vector perpendicular to the plane of incidence; in this case, the boundary conditions are identical) since both light and neutrons satisfy the same time-independent wave equation. Thus, on entering a material ($n < 1$) from vacuum ($n = 1$), neutrons will be 'totally externally reflected' for glancing incidence angles (measured from the surface) less than the critical angle

$$\theta_c \approx [2(1-n)]^{1/2} \approx \lambda(\rho a/\pi)^{1/2}, \tag{28}$$

which depends on the neutron energy. The neutron index can be rewritten as

$$n = (1 - U_{\mathrm{F}}/E)^{1/2}, \tag{29}$$

where E is the incident neutron kinetic energy. The effective potential U_{F} is between 100 and 300 neV (1 neV $= 10^{-9}$ eV) for most materials, giving $\theta_c \approx 17$ mrad $\approx 1^\circ$ for 2 meV (20 K thermal energy) neutrons.

3.1. Neutron polarization

A neutron polarizer can be made by applying a thin magnetized ferromagnetic film to a highly absorbing surface. Neutrons in the appropriate spin state will, through the Zeeman interaction $\vec{\mu} \cdot \vec{B}$, have a larger critical angle and be reflected while those in the other state will be transmitted by the film and lost in the absorbing surface. Such polarizers have become quite sophisticated and yield beam polarizations of better than 95%. Development of such mirror polarizers was a significant achievement; previously, neutron polarization was based on small angle scattering in bulk-magnetized iron. The transmission and polarization by this technique was at best marginal; Ramsey has some commentary on the subject [20]. More recently, optically pumped ^{3}He has been employed as a highly efficient neutron polarizer by use of spin-selective absorption.

With modest guiding magnetic fields, the neutron spin polarization for a neutron beam can easily be maintained if the neutron motion is so slow that the magnetic moment always keeps the same orientation with respect to the magnetic field $\vec{B}$ (adiabatic case). The necessary condition is that the time dependence of the field, as seen by the neutron moving through the inhomogeneous field, is much less than the precession frequency of the neutron moment in the field (taking τ as the characteristic time scale of the field change):

$$\frac{1}{\tau} = \frac{1}{B}\left|\frac{\mathrm{d}\vec{B}}{\mathrm{d}t}\right| \ll \frac{\vec{\mu} \cdot \vec{B}}{\hbar} = \omega_{\mathrm{L}}. \tag{30}$$

It is usually expected that, in this limit, the polarization loss is exponentially small (see [16], section 53), as described by the Landau–Zener equation.

An inhomogeneous magnetic field will exert a force on a neutron,

$$\vec{F}_{\mathrm{m}} = -\vec{\nabla}\vec{\mu} \cdot \vec{B} = \pm|\vec{\mu}|\vec{\nabla}|\vec{B}(\vec{r})|, \tag{31}$$

where, in the last equality, it is assumed that the adiabatic condition applies.

3.2. Production and moderation of neutrons

The earliest neutron experiments made use of radium–beryllium or polonium–beryllium sources, with neutrons being released in the reaction

$$\alpha + {}^9\mathrm{Be} \rightarrow {}^{12}\mathrm{C} + \mathrm{n}.$$

Cyclotrons can also be used as the α source, as was done in some early neutron magnetic moment experiments. At present, the most intense sources are nuclear reactors, with maximum available thermal (i.e., moderated to 300 K) neutron fluxes of order 10^{15} n/(cm^2 s). Spallation sources, based on the bombardment of a high atomic weight target by an intense GeV proton beam, are competitive with reactors for some applications and may become more so in the near future. This point will be further discussed later in relation to a possible future neutron EDM experiment.

The neutrons initially released in such reactions have energies in the range of a few MeV for reactors to about 100 MeV for spallation sources. In order for the neutron optics arguments

presented earlier to be valid, the neutron wavelength must be at least a few Å (interatomic spacing in solids), corresponding to energies less than 0.03 eV (= 30 meV). The fast neutron energy can be dissipated by scattering from light nuclei; this process was quite accidentally discovered by Fermi and coworkers in 1934 (see [21] for a detailed and anecdotal discussion of this discovery).

The basic idea of moderation is that if a liquid or solid material (a moderator) is placed close to the core of a nuclear reactor, and if the nuclei do not absorb neutrons and the material is of infinite extent, energetic neutrons will eventually come into thermal equilibrium with the moderator with a Maxwellian energy distribution, the temperature given by that of the moderator. This is because when an energetic neutron collides with a proton at rest, the initial kinetic energy on average is divided equally between the neutron and proton. Thus, after 10–20 scatterings, the neutrons released by fission or spallation approach zero energy, with a lower bound corresponding to the temperature of the moderator. Nuclei with higher mass are less effective in direct moderation, but are still useful, heavy water and graphite being two examples. In any real system, the moderator is of finite extent and also absorbs neutrons according to $1/v$, thereby distorting the Maxwellian spectrum; in most cases, however, it is useful to approximate the neutron spectrum as Maxwellian with a temperature slightly higher than that of the moderator.

The thermal equilibrium density of neutrons with velocities between v and $v + \mathrm{d}v$ is given by

$$\rho(v)\,\mathrm{d}v = \frac{2\Phi_0}{\alpha}\frac{v^2}{\alpha^2}\exp(-v^2/\alpha^2)\frac{\mathrm{d}v}{\alpha} \to \int v\rho(v)\,\mathrm{d}v = \Phi_0, \tag{32}$$

where Φ_0 is the total thermal flux which characterizes the strength of the neutron source, $\alpha = (2k_\mathrm{B}T_\mathrm{n}/m)^{1/2}$, and T_n is the neutron temperature.

There is a lower practical limit to the temperature that a neutron can achieve in moderation, regardless of how cold the moderator is. When the neutron energy becomes less than the vibrational energy levels in a solid (or liquid), the effective mass (in regard to neutron collisions) of the atoms that the moderator comprises becomes infinite, leading to a severe reduction in the rate of moderation. The effective neutron temperature of a liquid deuterium or hydrogen moderator maintained at 20 K is about 25–30 K. Other materials, such as solid methane, achieve similar neutron temperatures. Neutrons of this temperature, corresponding to a wavelength of about 6 Å or a kinetic energy of 3 meV, are usually referred to as cold neutrons (compared to 1.8 Å for 'thermal' (room temperature energy) neutrons).

For condensed matter studies, neutrons with just that energy are among the most interesting for inelastic scattering and structure measurements. For fundamental work such as EDM measurements, one would like the coldest possible neutrons to maximize the interaction time, for example, in a beam experiment. Fortunately, the cold neutron spectrum is close to a true thermal distribution, so there is in fact a substantial density of neutrons at lower energies. The art of neutron EDM experiments is in making efficient use of the lowest possible energy neutrons.

3.3. Transport of cold neutrons

Neutron guides, which are essentially evacuated pipes with the inner surface coated with a very smooth layer of high effective potential material, operate on the principle of total internal reflection [22]. The neutrons which diffuse from, for example, a 20 K liquid deuterium moderator, have their velocities isotropically distributed. If the entrance to a neutron guide is placed as close as possible to the moderator, then neutrons with velocities directed within a solid angle determined by the critical angle can be transmitted with very little loss over

distances of order tens of meters. Thus, guides provide a source of neutrons some distance from the moderator, but with a flux (within the solid angle) equal to that at the moderator surface. However, the primary advantage of a neutron guide is that it can be slightly bent; faster neutrons and γ rays directly from the reactor core pass through the walls of the guide, and can thus be separated from the experimentally useful slower neutrons which follow the guide in spite of its curvature. Such a separation reduces the experimental background and makes low-counting-rate cold-neutron experimental techniques possible. In fact, the success of the Institut Laue-Langevin in Grenoble, France, is due in large part to such careful shielding; here, the bent guides actually pass through a pool of water several meters long, the water serving as a nearly perfect shielding material.

3.4. Ultracold neutrons

Although the possibility of storing neutrons with low kinetic energy in material bottles is usually attributed to Fermi, Zeldovich was the first to take the idea seriously enough to put it into print [23]. The idea is that neutrons with kinetic energy $E < U_F$ will be reflected from the material surface for all incidence angles, and thus a storage bottle can be constructed. The reflection from the material surface is analogous to the total internal reflection of light. The storage lifetime can be long because the time that a UCN interacts with the wall (10^{-8} s) compared to the time between wall collisions (0.05 s) is very small.

Neutrons with such low velocities ($v < 7$ m s^{-1} for most materials corresponding to U of order hundreds of nano electron volts) are referred to as UCN because their average kinetic energy, as a temperature, is 5 mK or less. UCN production and storage are now well-developed technologies after some intense and difficult research over a 20 year period starting in the late 1960s [9].

UCN can be transported as a gas through pipes of high potential materials (stainless steel, for example). In addition, UCN can be polarized by transmission through a thin magnetically saturated foil; the foil material, typically a Fe–Co alloy, is chosen so that the saturation flux Zeeman shift just cancels the UCN potential for one spin state; that spin state passes easily through the foil while the other is reflected. It is also possible to polarized UCN by applying a magnetic field in a region of the guide; one spin state will gain energy on entering the field region, while the other state will not have enough kinetic energy to pass the region. A field of several Tesla is sufficient to fully polarize a UCN current, as has been demonstrated in a number of experiments.

UCN exist in the low-energy tail of the Maxwell–Boltzmann distribution, but their extraction from a moderator requires some special techniques as described in [9]. An important limitation is the absorption of UCN in the material windows that must hold a moderator in place, e.g., liquid deuterium. In order to mitigate the losses of UCN from imperfect window transmission,'vertical extraction' has been employed, where very cold neutrons (VCN) propagate vertically, becoming UCN at some height of a few meters, but their initial higher velocity reduces losses.

4. Comparison of experimental techniques

Over the last 60 years or so, a number of experimental techniques have been put forward to measure the neutron EDM; the only ones that have set significant limits have been based on magnetic resonance measurements. However, interest remains in the possibility of detecting a neutron EDM in a scattering experiment, the idea that the neutron can interact with an atomic-scale electric field which is five orders of magnitude larger than any conceivable laboratory

field. This paper will focus on the present upper limit of the neutron EDM and its prospects for improvement, with experiments that employ the storage of UCN. Other techniques will be mentioned to provide the motivation for the UCN experiments and their specific configurations.

All EDM searches are based on the application of an electric field and then searching for an appropriate response. In the case of magnetic resonance measurements, the value of the electric field is obvious, while in scattering experiments, determining the effective electric field is challenging. However, all experiments can ultimately be cast as measurement of the effective interaction energy of a neutron with an electric field: in the presence of a non-zero EDM, an electric Zeeman effect occurs in addition to the usual magnetic Zeeman effect, and the Hamiltonian of the system is

$$H = -(\mu \vec{B} + d_n \vec{E}) \cdot \frac{\vec{s}}{|s|}, \tag{33}$$

where $\vec{B}$ and $\vec{E}$ are the applied static magnetic and electric fields, μ is the magnetic moment, $s = 1/2$ is the net angular momentum of the neutron, and d_n represents the EDM.

The art of all EDM measurements is in the separation of spurious electric field effects from a true EDM effect. The spurious effects can be made quite small; this illustrates an advantage of EDM experiments over the T violation study involving β decay or neutron transmission [24], where the sought T violation signal cannot be turned on and off and appears alongside other allowed processes.

In writing equation (33), we have ignored, for example, changes in the internal structure of the neutron due to the application of the electric field (electric tensor polarizability). Also ignored is a possible static electric quadrupole moment; these two possible effects indicate some of the advantages of working with spin-1/2 systems, where the only possible (PT even) electromagnetic moment is the magnetic dipole. For a spin-1/2 system, there is no energy shift between $m_{\rm F} = \pm 1/2$ due to application of an electric field, and therefore no directly observable effect. Also we have assumed that the net species charge is zero, supposedly this is exactly true for the neutron.

A typical experimental observable is the change in Larmor precession frequency associated with a reversal of $\vec{E}$ relative to $\vec{B}$; this is an energy shift correlated with the quantity $\vec{E} \cdot \vec{B}$, a P- and T-odd quantity. An EDM of 1×10^{-26} e cm would produce a change in precession frequency, on reversal of $\vec{E}$ relative to $\vec{B}$, of 1×10^{-7} Hz when $E = 10$ kV cm^{-1}. This frequency shift corresponds to a magnetic field of about 2×10^{-11} Gauss for a neutron or diamagnetic atom, or about 10^{-13} Gauss for a paramagnetic atom. Given that the Earth's magnetic field is of order 0.5 Gauss, we see immediately that magnetic field control is crucial for any EDM experiment.

Other EDM observables are changes in position or momentum of a neutron interacting with an electric field gradient; such effects have been sought in neutron scattering experiments. The magnitude of the force $\vec{f}$ is simply given by the gradient of (33), and therefore the detection of an EDM force can ultimately be associated with an energy shift.

This leads to the definition of a figure of merit F for EDM measurements. From the uncertainty principle, the accuracy with which an energy change can be measured is inversely proportional to the time that the neutron interacts with a given electric field. The magnitude of the energy change is proportional to the effective electric field. Finally, the shot noise of the measurement is proportional to the square root of the neutron current I, leading to

$$F = ET\sqrt{I} \tag{34}$$

where, in the case of a neutron storage experiment, $I = N/T = \rho V/T$ where N is the total number of neutrons (product of density ρ and volume V) counted at the end of the

Table 3. Comparison of neutron EDM experimental sensitivities, where the systematic limit represents the control required to attain the full fundamental shot noise sensitivity.

Technique	E (V cm^{-1})	T (s)	I (n/s)	Sys. Lim.	$ET\sqrt{I}$
Bragg reflection	1×10^9	2×10^{-7}	10^4	$\theta_{EB} < 10^{-4}$	2×10^4
Neutron beam magnetic resonance	2×10^5	1.5×10^{-2}	1×10^6	$\theta_{EB} < 10^{-5}$	3×10^6
Ultracold neutron	1×10^4	100	250	$\delta E/E < 0.1$	2×10^7
Pendellösung (α-quartz)	2×10^8	2×10^{-3}	2×10^3	$\theta_{EB} < 10^{-7}$	2×10^7
UCN-^{3}He	5×10^4	500	5×10^3	$\delta E/E < 0.1$ $\partial B_0/\partial z < 0.01\ \mu$G cm^{-1}	2×10^9

measurement of duration T, assumed to be dominated by the coherence time. This factor allows us to compare different experimental techniques, as shown in table 3.

Because Bragg scattering experiments require the setting of an angle to a degree of precision that appears as experimentally impossible, we will not review this work here. Because the electric field in the crystal cannot be turned on and off, and detection and discrimination of an EDM effect requires absolute alignment of the crystal axes, the problem with these experiments are similar to those expected in neutron absorption or spin rotation experiments; see [24] for a discussion of the experimental issues.

5. Systematic effects in magnetic resonance experiments

5.1. $E \times v$ effects in beam experiments

Another spurious effect is the so-called motional magnetic field, first addressed in relation to a Cs atomic EDM experiment. Its effects are most severe for atomic beam experiments [25]. When one moves relative to the sources of a static electric field $\vec{E}$, according to special relativity, a magnetic field $\vec{B}_m$ is generated in the comoving frame which to first order in v/c is

$$\vec{B}_m = \vec{E} \times \frac{\vec{v}}{c}. \tag{35}$$

For a typical cold neutron velocity of $v = 1000$ m s^{-1} in an electric field of 100 kV cm^{-1}, $B_m = 1$ mG. Now consider an experiment where there is a large applied magnetic field $\vec{B}_0$ and an EDM is sought by measuring the shift in Larmor precession frequency on reversal of an electric field $\vec{E}$, as implied by (33).

If $\vec{E}$ and $\vec{B}_0$ are nearly parallel as shown in figure 2, and $B_m \ll B$, the effective magnetic field strength is given by the magnitude of $\vec{B} = \vec{B}_0 + \vec{B}_m$

$$B = B_0 + \theta_{EB} B_m + \frac{1}{2}\frac{B_m^2}{B_0}, \tag{36}$$

giving a change in Larmor frequency of

$$\delta\omega = \frac{\gamma\theta_{EB} v}{c} E + \frac{\gamma v^2}{2c^2}\frac{E^2}{B_0}, \tag{37}$$

where γ is the gyromagnetic ratio and θ_{EB} is the angle between $\vec{E}$ and $\vec{B}_0$ in the plane perpendicular to $\vec{v}$. If B is substituted into (33), it can readily be seen that if $\theta_{EB} \neq 0$, a

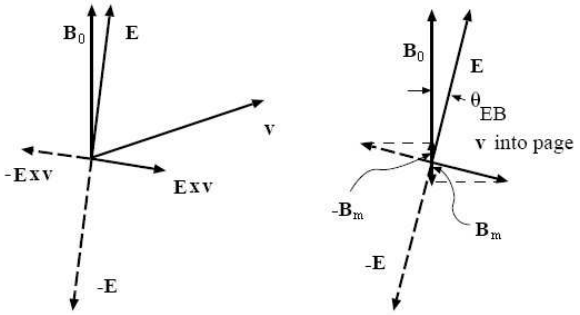

Figure 2. Geometrical picture of the $\vec{E} \times \vec{v}$ effective magnetic field, where $-B_{\rm m}$ is indicated in the figure.

spurious shift correlated with $\vec{E} \cdot \vec{B}$ is generated, which has the same signature as an EDM. However, this is not a true T violating effect, for under T, $\vec{v}$ reverses sign, and therefore so does $\vec{B}_{\rm m}$. The important point is that reversing $\vec{E}$ relative to $\vec{B}$ does not create the time-reversed Hamiltonian; $\vec{v}$ must also be reversed. Even in the case where $\theta_{\rm EB} = 0$, there is a relative shift quadratic in $B_{\rm m}$, which may require that the magnitude of E does not change significantly on reversal.

The limit on $\theta_{\rm EB}$ in the final beam experiment, performed in 1977 using the Oak Ridge apparatus that had been moved to the Institut Laue-Langevin, can be estimated as follows. The neutron velocity was about 100 m s^{-1}, implying a motional field of 0.1 mG. The reported uncertainty for this experiment is 1.5×10^{-24} e cm, implying a limit on the shift in a resonance frequency of about 20 μHz in 100 kV cm^{-1}, further implying a magnetic field control of about 10 nG, or a part in 10^5 of the motional field. Thus, the requirement on $\theta_{\rm EB}$ for the last neutron beam EDM experiment was $\theta_{\rm EB} < 10^{-5}$ radians. Although much effort was expended in dealing with this effect, which included mounting the entire experiment on a Navy Surplus gun turret in an attempt to cancel the $E \times v$ systematic by reversing $\vec{v}$ through the apparatus, it remained the ultimate limiting factor for neutron beam experiments. These techniques were abandoned in favor of ultracold neutron storage experiments which have the advantage that $\langle v \rangle = 0$ so the motional field is expected to have very small effects. We address these effects later in this section. Of course, $\langle v \rangle = 0$ requires that there not be a correlated flow of UCN or magnetometer atoms across the cell, due to, for example, persistent currents after filling. These effects have been considered and are generally thought of to be quite small.

5.2. Electric-field correlated magnetic effects

Whenever high voltages are applied to a system, small leakage currents invariably flow through insulators, and these currents generate magnetic fields which are correlated with the electric field direction and are indistinguishable from an EDM. The leakage current magnetic field is a function of the electric field and adds a term to the Hamiltonian (33)

$$H = -[\mu \vec{B} + \hat{z}(\beta \hat{z} \cdot \vec{E}) + {\rm d}\vec{E}] \cdot \vec{s}/|s|, \tag{38}$$

where β represents the average projection of the magnetic field generated by the current density

$$\vec{j} = \sigma \vec{E} \tag{39}$$

along the static magnetic field direction ($\hat{z}$), with σ representing the electrical conductivity. A non-zero β implies some helicity of $\vec{j}$ along $\hat{z}$.

The apparent T-odd character of this new term is the result of the irreversible 'macroscopic' process(es) which lead to (39). Also, under parity reversal, the helicity of the leakage path, hence the effective magnetic field, changes sign; under parity reversal, $\vec{E}$ also changes sign, so we see that the leakage current effect is even under parity reversal, unlike a true EDM.

For beam experiments where the insulators and conductors leading to the high voltage plates can be relatively well spatially separated from the sensitive measurement area, leakage current fields are not so troublesome as in the case of storage experiments where the cell walls generally serve a second purpose as the high voltage electrode spacer.

A worst-case scenario is when all the leakage current flows in a closed loop around the cell; given that such a current flow is highly unlikely, to estimate a possible systematic effect, one-quarter of the field at the center of a loop is sometimes taken. Note that if such a helical current existed due to some imperfection in the cell walls, reversing the cell orientation does not distinguish this effect because the leakage current helicity and hence magnetic field direction is a fixed property of the cell.

It is also important that the leads which supply the high voltage are coaxial with the leakage current return leads, otherwise the leakage currents, charging displacement currents when the electric field magnitude/direction is changed, or impulse currents associated with sparks can cause a systematic magnetization of the magnetic shields.

This discussion might appear as academic, but in fact two neutron EDM experiments, one at the Institut Laue-Langevin (ILL) in Grenoble, France, [26] and one at the Petersburg Nuclear Physics Institute (PNPI) in Gatchina, Russia, [27], reported results in the mid-1980s that were affected by systematics apparently of this type.

Of interest was the announcement of results from these two groups that were non-zero, agreed in sign and magnitude, and were at the 90% statistical confidence level. This announcement created a worldwide sensation. The problems with the data were found and reported in later publications [28, 29].

The quality of the data from the ILL experiment described in [28] is best illustrated in figure 3. In 1998, data from an improved neutron EDM experiment [32] (to be discussed later) were combined with the older data from 1990 [28] that were contaminated by magnetic field systematics associated with the application of voltage to the neutron storage cell. This figure was prepared for a subsequent analysis of the validity of combining new, systematic free data, with the old data that were limited in accuracy due to systematic effects. As can be seen in this plot, the data from the early experiment have a marked bi-modal character. In the data set, it was evident that major changes in the systematic EDM occurred whenever the measurement apparatus was disassemble and reassembled, usually for general maintenance. In the early analysis of the data of [28], it was assumed that if the average of the systematic magnetic field in the three rubidium magnetometers, shown schematically in figure 4, had zero average, the data set was systematic free. In fact, data selected by this criterion showed the largest neutron EDM. This is not surprising, as this selection of the data, where the average was near zero, made the experiment most sensitive to leakage currents in the neutron storage cell as the systematic field, due to helical leakage currents in the bottle, at the closest magnetometer was expected to be a factor of 2 larger than the outer two magnetometers, and of an opposite sign.

The problem was uncovered when the correlations between the individual magnetometer systematic magnetic fields (associated with application of the high voltage) and the neutron frequency were shown to be statistically significant, *invalidating any possibility of reliably detecting a non-zero neutron EDM at the level of the intrinsic sensitivity of the experiment*. The correlation technique is described in detail in [9] (section 7.3.4) and in [8] (section 4.5.2).

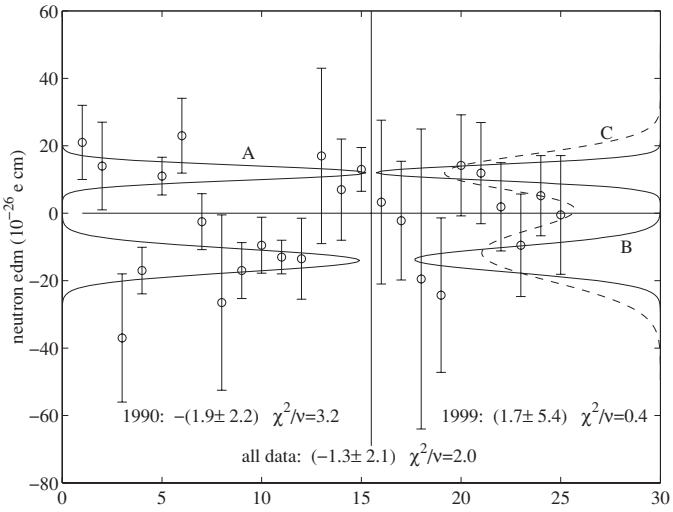

Figure 3. Distribution of neutron EDM values over the course of running the 1990 ILL experiment, shown in the left-hand plot labeled A. Each point represents several weeks of running, usually a complete reactor fuel cycle. The plot on the right side includes subsequently acquired data using the Hg comagnetometer system [30]. Given that the previous data set was demonstrably contaminated by systematic effects, the combining of the data sets was not statistically valid, as discussed in [31]. Curve B is the distribution assuming that the errors of the earlier data are systematic free, while curve C increases the error of the earlier data to reflect the systematic uncertainty, and there was no evident increase in sensitivity by combining the data sets.

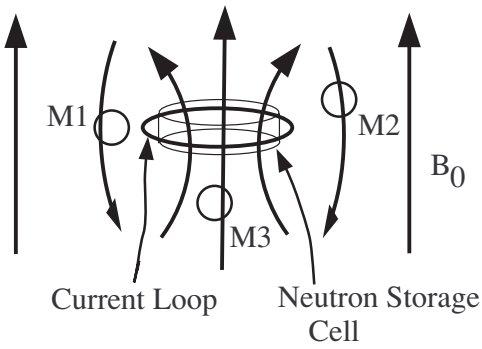

Figure 4. The external magnetometer problem. Leakage currents associated with the application of a high voltage to the measurement cell can flow in a loop (or some fraction thereof) around the cell, creating a magnetic field that is correlated with the direction of the electric field. Depending on the location of a magnetometer, the field from the loop can add or subtract to the applied static field B_0.

The point in discussing this problem in such details is that there are several planned or ongoing experiments that do not employ a so-called 'comagnetometer'. Results from these experiments will need to be considered with the utmost caution, for as we know that the past is usually prologue. However, we do point out that the most accurate EDM measurement to date, the Seattle ^{199}Hg experiment, did not have a comagnetometer, but relied on the use of four measurement cells in very close proximity. As discussed in [8], (equation (3.37)), the leakage current systematic scales as the radius of the storage cell, as do displacement current

systematics. In [8], it is suggested that a systematics will be an issue at the level of 3×10^{-28} e cm for the ^{199}Hg experiment, which after a heroic effort produced a limit an order of magnitude better. In comparison, the typical UCN storage cell has radius 10–20 times larger than the cell used in the ^{199}Hg experiment, and in addition the neutron magnetic moment is four times larger than the ^{199}Hg magnetic moment. Based on this comparison, the prospects of attaining a neutron EDM limit in the 10^{-27} e cm range without a comagnetometer appear as dismal.

5.2.1. The Ramsey comagnetometer. With the increased sensitivity offered by the use of ultracold neutrons (UCN) in neutron EDM experiments, it became evident very early that magnetic field noise and systematic effects would ultimately limit the experimental sensitivity. Although the ideas had been discussed, the first published analysis of an *in situ* magnetometer was given by Ramsey [33]. The idea is that a spin polarized atomic gas can be stored along with the UCN in the same volume and serve as a magnetometer. To very high accuracy, the atomic magnetometer can provide a measure of the magnetic field directly experienced by the UCN. The ambiguity associated with external magnetometers is thus eliminated.

Such an *in situ* magnetometer is referred to as a comagnetometer. This term appears to have been invented in the late 1980s by Professor N Fortson's group at the University of Washington. Identification of a comagnetometer for a specific EDM experiment is a sort of experimental Holy Grail. Finding such a magnetometer provides a measure of guarantee for the success of an experiment.

Ramsey's analysis addressed the use of polarized ^{3}He atoms. In his analysis, he shows that the direct effects due to field gradients and non-resonant radio-frequency pulses on the spin precession frequency are small for conditions normally found in UCN EDM experiments. Because these background effects are not correlated with application of the high voltage, they produce no intrinsic systematic effect. It was believed that the $\vec{E} \times \vec{v}$ field would be zero for a stored UCN experiment because the average value of v is effectively zero. However, recently it has been realized that a quadratic effect persists which places requirements on the accuracy with which the applied voltage must be reversed. More important is the very recent realization that a quantum interference between a magnetic gradient and the $\vec{E} \times \vec{v}$ field can cause a systematic effect. These problems are discussed later in this section.

Ramsey discusses the requirement that the comagnetometer species does not have an EDM of its own. For light diamagnetic atoms, a nuclear EDM is suppressed by $\alpha^2 Z^2$ ($\alpha = 1/137$ is the fine structure constant and Z is the atomic number) due to shielding by the electron cloud.

Despite several years of research with promising results at the University of Sussex, a practical ^{3}He magnetometer did not appear feasible. Eventually, optically pumped ^{199}Hg was successfully employed as a comagnetometer in the ILL experiment, to be discussed later in this paper.

Because UCN have velocity less than 7 m s^{-1} or so, their spatial density in a finite-size storage cell is significantly modified by the earth's gravitational field. There is a considerable shift in the center of mass between a UCN gas and an atomic gas in the gravitational field, due to the difference in their effective temperatures [33]. Although the UCN gas does not strictly represent an equilibrium system, we can estimate the downward displacement by assuming an effective UCN temperature of 2.5 mK;

$$\Delta h = -\frac{h}{2} + \frac{1}{h}\int_0^h x\, \mathrm{e}^{-m_\mathrm{n} g x/kT}\, \mathrm{d}x \approx -\frac{m_\mathrm{n} g h^2}{3kT}, \tag{40}$$

where h is the cell height. For a 20 cm cell, the displacement is on the order of 6 mm. For the higher temperatures of the magnetometer gas, the shift is comparatively insignificant.

Although this displacement represents an imperfection in the monitoring of the exact magnetic field as seen by the UCN, the discrepancy is small. A systematic magnetic shift that failed to be corrected would most certainly be evident in the direct UCN or atomic magnetometer signal, provided that the background magnetic field noise is sufficiently small.

It is generally assumed that for a comagnetometer to be useful, the time to average the magnetic field over the entire storage volume is shorter than the spin coherence or total measurement time. If this averaging time is too long, there will be a relaxation (decoherence) effect unless the magnetic gradient is sufficiently small. Quantitatively, the experiment should be operated in the 'motional narrowing' limit, where the inverse of the gradient-induced frequency shift is small compared to the time for a spin to diffuse across the storage cell. The dimensionless parameter d [34],

$$d = \left[\frac{2D}{L^2}\right]\left[\frac{\gamma GL}{2\pi}\right]^{-1} \gg 1 \tag{41}$$

in the motional narrowing limit, where D is the diffusion coefficient, L is a maximum characteristic length in the system, γ is the gyromagnetic ratio and G is the magnetic field gradient. The first term in the brackets is the rate that a spin moves diffusively through the entire cell, and the second term is the characteristic dephasing time associated with a spatial static magnetic field gradient. As will be discussed later, when the gradient is small enough for the 'geometric phase' EDM to be small, d will tend to be large, for any imaginable D. However, a large d is a necessary but not sufficient requirement to reduce a possible EDM systematic gradient magnetic field (generated when an electric field is applied), and any particular system will require evaluation of its immunity to such effects. As will be discussed later, the fluctuating magnetic field due to the $E \times v$ motional field can also lead to relaxation [35].

A finite averaging time can lead to a systematic effect if the application of an electric field creates a voltage–polarity-dependent magnetic field gradient and if there is a position dependent detection/measurement sensitivity. These types of problems have been discussed in relation to the ^{199}Hg EDM experiment [36]. The effect can be visualized as follows. Consider a cell of long spatial extent, with the spins detected only at one end (the 'near' end) of the cell. Assume also that the systematic gradient only appears at the 'far' end. In the limit where the comagnetometer diffusion time becomes extremely long, the comagnetometer, because of the spatial sensitivity to the detection, will not register magnetic fluctuations at the 'far' end of the cell, while UCN, not being hindered by diffusion, will sample the entire cell relatively rapidly. Thus, a second criterion for a comagnetometer to be effective is that the combination of diffusion time and of detection position sensitivity variations both be small so that the cell is uniformly averaged by both the UCN and comagnetometer species to an adequate degree of precision.

Another comagnetometer imperfection results from the so-called pseudomagnetic field. This field results from the spin-dependent coherent scattering cross-section, which leads to an energy shift for the UCN that is spin dependent and thus appears as a magnetic field. The pseudomagnetic field is not directly affected by the application of an electric field, but can be the source of precession frequency fluctuations and hence extra noise in the system. The magnitude of the pseudomagnetic field can be reduced by ensuring that the magnetometer spins have no component along the static magnetic field, which is possible by careful control of the spin flip pulses.

Such pseudomagnetic fields have appeared in other EDM experiments, for example, a ^{129}Xe experiment [37] where the field was of order 1 mHz due to the presence of spin polarized rubidium that was used to polarize and detect the ^{129}Xe spin precession. This frequency, as an

EDM in a 5 kV cm^{-1} field that was used in the experiment, corresponds to 10^{-22} e cm, while the final experiment sensitivity is in the 10^{-26} e cm range. This level of discrimination results simply from the fact that the electric field does not directly affect the pseudomagnetic field, and the spin of the rubidium was approximately orthogonal to the applied static magnetic field.

A final concern is the possibility that the magnetometer atom could stick to the wall for a significant period of time compared to the time that a UCN interacts with a wall (i.e., the time for quantum reflection, which is of order 10^{-8} s). For a heavy atom like Hg, together with the known binding energy of 0.1 eV on typical surfaces, implies a sticking time of order 10^{-6} s, which can be calculated by considering the density of states on the two-dimensional surface compared to the density of states for the atom freely propagating in the storage cell. Estimates for the ILL Hg comagnetometer experiment suggest that this effect, which would lead to a difference in the spatial averaging of the magnetic field by the UCN compared to the Hg, is very small. However, improvements in the experimental limit for the neutron EDM using this technique beyond 10^{-27} e cm will require a careful study. Also of concern is a modification to the diamagnetic correction of the atom during its dwell on the wall, the idea being that the electron density at the nucleus is affected by the interaction with the storage container walls. Since the diamagnetism results from the inner electrons, this effect is expected to be quite small.

As a final note in this section, the use of a comagnetometer versus external magnetometry offers a final and critical advantage. For external magnetometry, as shown in figure 4, the total magnetic noise registered by the magnetometer is the combined noise due to the magnetometer itself, and that due to external noise fields resulting from imperfections in the magnetic shielding. This total noise must be low enough so that a high voltage correlated shift in the magnetic field can be detected with the same accuracy as the neutron resonance signal. Therefore, it is difficult to use external magnetometers as 'an extra layer of magnetic shielding' to compensate for the limited performance of a magnetic shield, as this requires a nearly impossible level of magnetic shielding to attain a level of accuracy for correlated magnetic field measurements below an EDM sensitivity of 10^{-26} e cm.

As an example, the ILL UCN experiment [28] employed three Rb magnetometers near the UCN storage cell. These magnetometers had net sensitivity just at the limit to be useful to detect and eliminate a systematic magnetic field change. The sensitivity was limited by the intrinsic magnetometer sensitivities, but mostly by magnetic field noise due to the finite shielding ability of the magnetic shields. When this experiment was rebuilt, incorporating a ^{199}Hg magnetometer, the innermost magnetic shield layer was removed (this experiment is discussed later in this paper). As a consequence, the magnetic field noise due to external sources was so large that the Rb magnetometers were useless in detecting possible small field changes, at the level of sensitivity of the neutron EDM frequency change, that one would hope to potentially detect with application of the high voltage. However, the ^{199}Hg magnetometer could be used to correct for field fluctuations, and even if the high-voltage fluctuations could not be discriminated from the external noise, there is a reasonable degree of assurance that the systematic fields were corrected along with the other fluctuations. In fact, the degree of correction can be tested by applying arbitrarily pathological magnetic gradients to the system, and then scaled to what could be reasonably expected from leakage currents, etc. Up to now, no specific studies have been performed, but the apparent performance of the ^{199}Hg magnetometer suggests at the present limit, the degree of perfection is adequate.

In the following sections, we will describe newly discovered systematic effects due to the $\vec{E} \times \vec{v}$ generated magnetic field that affects mostly the comagnetometer atoms and represents the final known imperfection. These are the effects that can be controlled, but as we will discuss, require a careful experimental design.

5.3. $E \times v$ effects in storage experiments

5.3.1. Quadratic effect. Although the motional field is most significant in the case of beam experiments, examples of which are the early neutron EDM experiments and the more recent thallium EDM experiment, [38] there can be some subtle effects in other cases. EDM experiments using optically pumped atoms or neutrons contained in a cell have on average $\vec{v} = 0$ simply because the atoms are free to rattle about the cell, so one might expect that there is no net motional effect. However, as we will show, the fluctuating field associated with the random velocity can in fact lead to sizable systematic effects; the term quadratic in v in $B = \sqrt{B_0^2 + B_{\rm m}^2}$ in the effective magnetic field persists even if the average velocity is zero, and one may wonder why it is possible to measure EDMs to the achieved levels of sensitivity. If we consider a case where $B_0 = 10$ mG, and $v = 120$ m s^{-1}, $E = 10$ kV cm^{-1} as in the case of the ^{199}Hg comagnetometer used in the current Institut Laue–Langevin experiment, the quadratic term amounts to about 50 nG, corresponding to a shift of 35 μHz for the optically pumped and detected ^{199}Hg. The experimental accuracy is at the level of 10^{-7} Hz, which implies a magnetic field of about 0.1 nG, and would seem to require an electric field magnitude reversal symmetry of 1 part in 10^3 for an apparent ^{199}Hg EDM to be below the experimental limit.

An important point has been neglected in this estimate. In fact, the motional magnetic field is randomly fluctuating, and it simply is not correct to take the average square of this field. The motional field has a definite magnitude only for a time interval $\tau_{\rm c}$, the time between substantial velocity changes due to, for example, collisions with buffer gas molecules or cell walls. The parameter $\tau_{\rm c}$ depends on the system geometry, nature of the collisions and velocity of the particles.

For a spin-1/2 system, the net effect of the randomly fluctuating field can be readily quantitatively calculated in the context of the density matrix [39]. The Hamiltonian can be separated into static and time-dependent components

$$H = H_0 + H(t) = -2\pi\gamma\sigma_z B_0/2 - 2\pi\gamma f(t) B_{\rm m}\sigma_x/2, \tag{42}$$

where γ is the gyromagnetic ratio (Hz/G), $\sigma_{x,z}$ are Pauli matrices and $f(t)$ represents the fluctuating character of $B_{\rm m}$. Here we only consider the possibility of an x component of $B_{\rm m}$, but this does not change the result significantly. Eventually, both time and ensemble averages of the effect of this Hamiltonian must be determined.

By transforming into a rotating frame, the static component of the Hamiltonian can be eliminated,

$$H' = {\rm e}^{{\rm i}\omega t\sigma_z} H(t)\, {\rm e}^{-{\rm i}\omega t\sigma_z} = -2\pi\gamma f(t) B_{\rm m} D_z(\omega t)\sigma_x D_z(-\omega t), \tag{43}$$

where $\omega = 2\pi\gamma B_0$ and D_z is the spin-1/2 axial rotation matrix.

The effect of H' on the system is most readily calculated in a density matrix formalism, as discussed in [40] and [41]

$$\frac{{\rm d}\rho}{{\rm d}t} = \Gamma\rho = -\left\langle \int_0^\infty [H'(t), [H'(t-\tau), \rho]]\, {\rm d}\tau \right\rangle_{\rm av}, \tag{44}$$

where ρ is the 2×2 spin-1/2 density matrix and the average is over a time much longer than $\tau_{\rm c}$; also assumed is an average over the statistical ensemble represented by the subscript 'av'. This result comes from the second-order perturbative approximation to the density matrix evolution (see [40], chapter VIII, equations (28)–(32)). Γ is referred to as the relaxation matrix.

The double commutator in the integrand is proportional to the autocorrelation function of $f(t)$, which can be taken as a simple form

$$f(t)f(t-\tau) = \begin{cases} 0, & \text{if } \tau > \tau_c \\ 1 - \tau/\tau_c & \text{otherwise,} \end{cases} \tag{45}$$

where τ_c is the time between velocity changing collisions.

Ignoring exponential terms with arguments $\omega(\tau + 2t)$ gives

$$\Gamma_{11} = \Gamma_{22} = -\left\langle \frac{(2\pi\gamma B_m)^2}{2} \frac{1-\cos\omega\tau_c}{\omega^2\tau_c} \right\rangle_{av} \tag{46}$$

for the diagonal elements of the relaxation matrix, and for the off-diagonal elements,

$$\Gamma_{12} = \Gamma_{21}^* = -\left\langle \frac{(2\pi\gamma B_m)^2}{2} \left(\frac{1-\cos\omega\tau_c}{\omega^2\tau_c} + i\,\frac{\omega\tau_c - \sin\omega\tau_c}{\omega^2\tau_c} \right) \right\rangle_{av}. \tag{47}$$

The real components of Γ represent the spin relaxation, while the imaginary components of the off-diagonal elements represent a frequency shift; it is

$$\delta\omega = 2\pi f_m = \frac{1}{2}\left\langle (2\pi\gamma B_m)^2 \frac{\omega\tau_c - \sin\omega\tau_c}{\omega^2\tau_c} \right\rangle_{av}. \tag{48}$$

It is interesting to consider the limiting forms of (48). When $\omega\tau_c \gg 1$, the term $\sin\omega\tau_c$ has zero ensemble average (given a reasonably broad velocity distribution). Furthermore, taking into account the fact that $\vec{v}$ is not constrained to lie in a plane perpendicular to $\vec{E}$, $B_m \to B_m \sin\theta$ must be averaged over all possible directions on a sphere, giving a mean square effect $2B_m^2/3$. Thus, in the limit $\omega\tau_c \gg 1$,

$$f_m = \tfrac{1}{3}(\gamma B_m)^2/f_0 = \tfrac{1}{3}(\gamma vE/c)^2/f_0, \tag{49}$$

where $f_0 = \gamma B_0$. It should be noted that in this limit the shift does not depend on τ_c, and is the average quadratic expansion of the sum of the motional and applied magnetic fields as used in the estimate above. Measurements on stored ultracold neutrons operate in this regime.

In the case where $\omega\tau_c \ll 1$, the $\sin\omega\tau_c$ term can be expanded,

$$f_m = \frac{(2\pi)^2}{9}(\gamma B_m)^2 f_0 \tau_c^2 = \frac{(2\pi)^2}{9}(\gamma vE/c)^2 f_0 \tau_c^2, \tag{50}$$

where B_m and τ_c represent appropriate ensemble averages. The behavior here is rather unexpected in that the shift increases with f_0, which is opposite to the previous case. Any EDM experiment which employs a buffer gas operates in this regime as does a relatively fast moving comagnetometer.

The conclusion for the most recent ILL experiment is that the quadratic motional effect for the ultracold neutrons (velocity 5 m s^{-1}) is small enough to be of no concern. The effect on the ^{199}Hg is suppressed by a factor $(f_0\tau_c)^2 = (10\,\text{mG}\,0.759\ \text{Hz mG}^{-1}\,0.4\,\text{m}/120\,\text{m s}^{-1})^2 \approx 10^{-3}$ so is also negligible.

For the ^{3}He comagnetometer experiment that will be discussed later, the spin relaxation rate (real part of the relaxation matrix) is large enough to be of some concern for that experiment and provides a limit on the static magnetic field and coefficient of diffusion, D [35].

5.3.2. 'Geometric phase' effect. It is interesting to note that after 60 years of searching for an EDM of elementary particles a new effect can emerge. While this effect was unimportant for earlier searches it proved to be important for the most recent experiment and will be crucial for the next generation of experiments.

The effect of a time-varying magnetic field generated from the $E \times v$ motional field, in the context of Berry's geometric phase, was first put forward by Ramsey in connection with the

neutron EDM [42]. The principal idea is that the fluctuating $E \times v$ field causes the magnetic field to trace out a solid angle, and by Berry's analysis, this solid angle is proportional to a relative phase shift between the two spin sublevels, hence an apparent Larmor frequency shift. However, it was immediately recognized that Berry's phase alone is not sufficient to generate a non-zero-average effect. Later, this effect was analyzed by Commins [43] in connection with an electron EDM (thallium) beam experiment, who discovered that the presence of magnetic field gradients together with Berry's phase from the $E \times v$ field can give a frequency shift that is linear in the applied field. Due to a hint from Hunter [44], the effect was rediscovered in the most recent UCN storage experiment at the ILL [45]. Commins gives a very clear description of the effect valid for slowly varying fields and shows how it can be understood as a manifestation of Berry's geometric phase [46].

Another approach to the basic idea can be seen as follows [45]. Consider a case where, in a storage experiment, there is a radial magnetic field, proportional to r, due to a magnetic field gradient in the z-direction (B_0, the quantization axis, and the electric field E are along z). Now consider roughly circular orbits (never mind how this might be established), due to specular reflection around the bottle at a constant angle, in the x–y plane with radius approximately the bottle radius R. The wall collisions occur at a frequency of $1/\tau_c$ while the orbital frequency is $\omega_r = 2\alpha/\tau_c$ where α is the incidence angle relative to the surface. We can transform into a rotating frame at ω_r (note that this is not the Schwinger rotating frame that eliminates B_0) so that the problem is quasi-static [47].

The radial field, with the barrel gradient plus $v \times E$ field, is

$$B_R = B_r \pm B_E = aR \pm \frac{\omega_r R E}{c}$$

where $B_r(r) = (r/2)\,\partial B_z/\partial z = ar$ is the radial field due to the axial gradient, $\pm B_E = r\omega_r E/c$ is the radially directed $v \times E$ field, and $\pm$ refer to the rotation direction.

In the rotating frame,

$$B^2 = (B_0 - \omega_r/\gamma)^2 + (B_R)^2$$

where γ is the gyromagnetic ratio. Expanding in the limit where $B_R \ll B_0$ with transformation back to the lab frame we find

$$B = B_0 + \frac{1}{2}\frac{(aR - \omega_r RE/c)^2}{B_0 - \omega_r/\gamma} = B_0 - \frac{(aR^2\omega_r E/c)}{B_0 - \omega_r/\gamma}$$

keeping only terms linear in B_E. Averaging over the rotation direction (e.g., the sign of ω_r), the net effect of the gradient field combined with a $v \times E$ yields a systematic (magnetic field) shift of

$$\delta\omega = \gamma\delta B = -\frac{\gamma^2 a v^2 E}{c\left(\omega_0^2 - \omega_r^2\right)} \tag{51}$$

equivalent to equation (18) of [45]. Taking the limit $\omega_r/\gamma \ll B_0$ we have

$$\delta B = -\frac{aR^2\omega_r^2 E}{\gamma c B_0^2}, \qquad \delta\omega = -\frac{aR^2\omega_r^2 E}{cB_0^2} \tag{52}$$

which would seem to set the scale of the effect and is equivalent to equation (19) of [45]. In this limit, the frequency shift does not depend on γ, implying that it is the result of a geometric effect.

In the other limit, where the rotation frequency is much faster than the Larmor frequency, we similarly find that

$$\delta B = \gamma a R^2 E/c, \qquad \delta\omega = \gamma^2 a R^2 E/c, \tag{53}$$

which is independent of the motional frequency ω_r of the opposite sign from the previous limit and equivalent to equation (21) of [45].

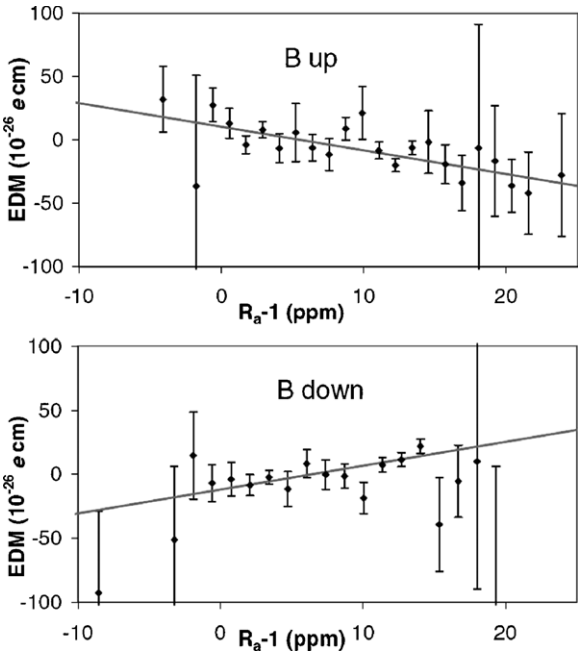

Figure 5. Apparent neutron EDM versus UCN-Hg frequency deviation from [48].

This effect was rediscovered in the context of EDM searches using stored UCN by Pendlebury *et al* [45], who found a correlation between the values of an apparent EDM in their data and the ratio of the precession frequencies of the UCN and the Hg comagnetometer. The data are shown in figure 5.

The manifestation of a systematic effect in these data results from a displacement of the centers of mass of the UCN and Hg distributions, with the UCN displaced by gravity by $\Delta h \leqslant 3$ mm (see equation (40)) along the z-axis. In the presence of a gradient $\partial B_0/\partial z$, the two species will see slightly different average magnetic fields and have slightly different Larmor frequencies. Defining, as in [45],

$$R_a = \frac{\omega_n/\gamma_n}{\omega_{Hg}/\gamma_{Hg}} \tag{54}$$

it is easy to see that

$$\frac{\partial B_0/\partial z\,|\Delta h|}{B_o} = \pm\,(R_a - 1)\,, \tag{55}$$

where the plus sign is for B_0 pointing down. Thus, $(R_a - 1)$ is a measure of the z-gradient and according to (52) and/or (53) we should expect an EDM signal proportional to this quantity. The slope in figure 5 agrees very well with this equation. After discovering this systematic variation in their data, Pendlebury *et al* undertook a detailed study of the effect in order to understand and correct for it, using the low- and high-frequency limits. They then went on to solve the Bloch equations for the motion of the spin in the combined electric and gradient magnetic fields, for the case of a single specularly reflecting orbits with no collisions, giving an expression for the systematic effect. They also studied the effects of collisions by means of extended numerical simulations of the Bloch equations.

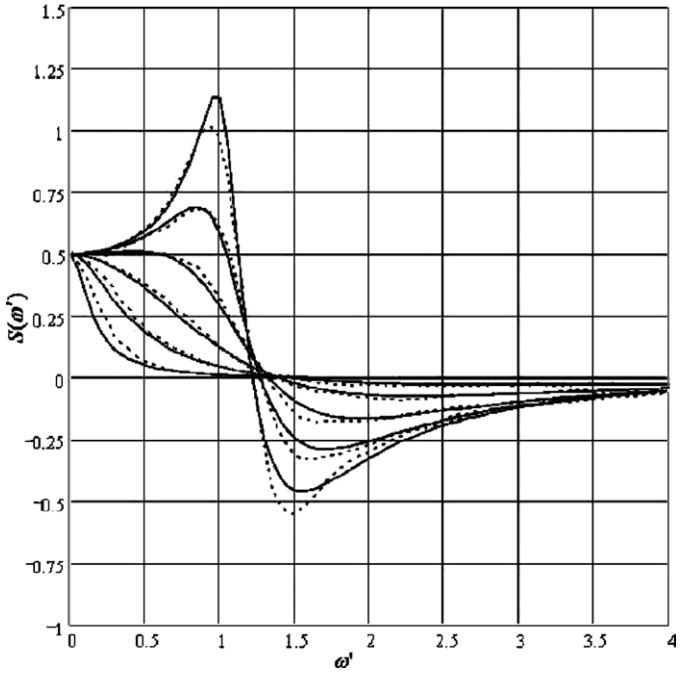

Figure 6. Normalized frequency shift for a constant velocity as a function of normalized applied frequency $\omega' = \omega_0 R/v$, for different values of the damping parameter $r_o = R/\lambda$. Solid curves: results of the analytic function, [50], equations (43) and (44). Dotted lines: numerical simulations from [50]. Starting at highest peak, $r_o = 0.2,\ 0.5,\ 2,\ 4,\ 10$ (cylindrical cell).

Further study of the problem [49] led to the recognition that the frequency shift is given by the spectrum of the velocity-position correlation function and hence can be derived from knowledge of the velocity correlation function averaged over the ensemble of particle trajectories. Rather simple analytic forms of the correlation function for the case of a single velocity and specular wall collisions have been obtained, for both cylindrical [50] and rectangular cells [51], but work considering velocity distributions and gas collisions has been both numerical and analytic, and necessarily depends on the size of the storage cell.

Figure 6 (dotted lines) shows the correlation function for a cylindrical measurement cell with specular wall reflections for different collision mean free paths λ, obtained from numerical simulations. The solid curves show the same results obtained from an analytical form of the correlation function [50] Solution agrees with the result obtained by the direct solution of the Bloch equation (equation (78), [45]) for this case. For values of $\omega_0 \gg \omega_r$, the velocity auto-correlation function is given by $e^{-\tau/\tau_c}$ with τ_c being the collision time. This region, where the shift $\propto 1/\omega_0^2$, is appropriate for stored UCN. For the opposite limit (long-time limit of the correlation function) appropriate for heavier comagnetometer atoms, e.g. Hg, the effect is generally larger as can be seen from the figure. The analytic result obtained in [50] is valid in the intermediate region as well. It is interesting to explore the possibility of using the zero crossing in this region to reduce the effect. In the case of a comagnetometer consisting of ^{3}He atoms moving in superfluid He^4, as in the experiment under development for operation at the Oak Ridge National Laboratory Spallation Neutron Source, the collision mean free path

is strongly temperature dependent and this can be used to tune the effect around the zero crossing, as has been described in [50].

As a final note, because the magnetic moments of the neutron and Hg atoms have opposite signs, the two species are precessing in opposite directions during the ILL measurement. It follows that the Earth's rotation will shift the two precession frequencies in opposite directions [52]. The laboratory is essentially a rotating frame, rotating with $\omega_\oplus = 2\pi/24\,(3600) = 2\pi\ (11.6\ \mu\text{Hz})$, so that a term

$$-\left(\frac{\omega_\oplus \sin\theta_L}{B_o\gamma'}\right) \tag{56}$$

should be added to the right side of (55), which would correspond to an EDM shift of $d_{n\oplus} = -2.57 \times 10^{-26}\ e$ cm, a non-negligible shift given the limit fixed by the experiment ($|d_n| < 2.8 \times 10^{-26}\ e$) cm. However it turns out that this effect was fortuitously almost exactly canceled, better than 15%, by the change of stray quadrupole magnetic fields on reversing the field, B_o [53, 54]. We note that this effect only occurs when equation (55) is used to obtain the field gradient.

6. Present experimental limit: UCN experiment with ^{199}Hg comagnetometer

Because both the ILL [28] and the PNPI [29] UCN EDM experiments were no longer limited by counting statistics but by magnetic systematics, it was decided to rebuild the ILL apparatus and include a comagnetometer, as we have already discussed, and thus provide a nearly exact spatial and temporal average of the magnetic field affecting the neutrons over the storage period. The use of polarized ^{3}He had already been considered [33], but the extreme difficulty in the detection of the ^{3}He polarization made its use in this context impractical.

The use of ^{199}Hg was suggested in 1986 [55] and is described in [56]. The advantage is that ^{199}Hg can be readily directly optically pumped and its polarization optically detected with 254 nm resonance radiation. Because ^{199}Hg is a $^1S_0$ atom, its ground state polarization is specified by the nuclear angular momentum, which is 1/2 for ^{199}Hg. In addition, the room temperature vapor pressure of Hg is more than adequate to provide the necessary density.

Of course, to be useful for a comagnetometer, it must be demonstrated that the chosen atomic species does not have an EDM of its own which could possibly mimic or mask a neutron EDM; in the case of ^{199}Hg, experimental limits were set at the level of sensitivity needed [57]. In these experiments, ground state spin-polarization lifetimes in excess of 100 s were routinely achieved in cells of about 5 cm^3 volume, even in the presence of electric fields up to 15 kV cm^{-1}. However, these cells included 250 torr of nitrogen to improve the high-voltage stability.

An unfortunate disadvantage of ^{199}Hg is that the walls of the container must be specially prepared to have long spin relaxation times. In all previous experiments, hydrocarbon waxes were used; these of course would be unusable with UCN. In addition, the wall coating has to be stable under the application of high voltage in vacuum since a high-pressure background gas cannot be used with the UCN. A fused silica insulating ring 20 cm high separating two diamond-like carbon coated aluminum plates was used as the storage cell, with a total volume of 20 l.

A schematic of the experimental apparatus is shown in figure 7. To increase the experimental sensitivity through storage time and UCN number increases, a 20 l volume storage bottle was constructed, compared to 5 l in the earlier version. The magnetic shields were the same as those used in the previous ILL experiment, only the innermost layer was

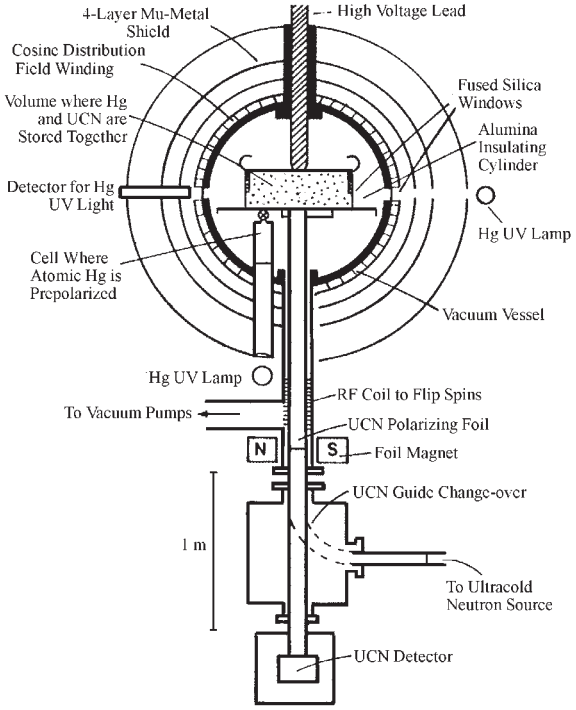

Figure 7. Schematic of the ILL UCN EDM experiment incorporating a ^{199}Hg comagnetometer.

removed. The loss in shielding factor was to be made up for by the improved volume comagnetometry.

In addition, there was a safety consideration for the use of Hg, and it was necessary to isolate the experiment with a gas-tight window which can withstand atmospheric pressure. The thin foil polarizer was redesigned to also serve as the window, with iron evaporated onto an aluminum foil. To account for the fairly high effective potential of the aluminum, after passing through the foil the UCN rise about 1 m. Tests were performed to determine the optimum height to maximize the number of UCN left in a test bottle after a 100 s storage period.

Provisions were included for polarizing the atomic vapor; an optical pumping cell was connected to an isotopically enriched Hg reservoir, a few milligram of HgO powder in a tube held at about 250 °C. This provided a current of ^{199}Hg atoms and could be controlled with a valve. The Hg was optically pumped to the appropriate spin state, parallel to the static field, with circularly polarized light from a Hg discharge lamp. After the Hg had been polarized, and after the storage vessel had been filled with polarized UCN, the neutron valve was closed; then polarized Hg was admitted to the neutron bottle. $\pi/2$ pulses were applied first for the ^{199}Hg and then for the UCN (the ^{199}Hg magnetic moment is about one third of the neutron magnetic moment). The free precession of the Hg spin was observed with a beam of circularly polarized resonance light which propagates across the bottle diameter, through the fused silica insulating cylinder. The storage vessel spatial average magnetic field, averaged over the measurement time, could be determined from the free precession signal.

At the end of the storage period, the second neutron pulse was applied, the bottle door opened, and the neutrons were counted and the final polarization state, hence resonant frequency, was determined as before. The Hg was pumped away during the UCN counting

period. While the storage was in progress, more Hg had been admitted to the optical pumping cell and polarized; the process was thus ready to be repeated.

An EDM would be evident from a change in the ratio of the magnetic moments between reversals of the electric field. Although the sensitivity of the Hg to a magnetic field is only 1/3 that of the neutron, the high signal-to-noise inherent in the free precession signal was a compensating factor, and the determination of the average field was a factor of 3 to 10 higher in sensitivity than the neutron accuracy and hence contributed very little noise to the measurement. The final uncertainty for this experiment, based on the shot noise, is about 3×10^{-26} e cm (95% conf.).

The figure-of-merit (equation (34))

$$F = \alpha E \sqrt{\rho V T},$$

where T is the coherence time, V is the storage volume, ρ is the UCN density, E is the applied electric field and α is the polarization factor, for this version of the experiment compared to the 1990 version is

$$F'/F = (.5 \times 4.5 \times \sqrt{0.7 \times 20000 \times 120})/(.6 \times 10 \times \sqrt{3 \times 5000 \times 80}) = .45$$

with the reduction in F largely due to the reduction in electric field strength. The larger volume compensated for the loss of UCN number density due to the relatively low potential of the fused silica/diamond-like-carbon storage cell of 110 neV (due to the fused silica), compared to 240 neV for Be/BeO used in the previous experiment, representing a loss in density by a factor of $(110/240)^{3/2} = 1/3$, compared to a factor of 1/4 in the experiment, with the additional loss due in part to a less transmissive polarizer.

7. Present experimental development

7.1. Hg comagnetometer experiment at PSI

The success of the Hg comagnetometer suggests that this technology should not be abandoned. Thus, the present plan is to upgrade the experiment and move it to a more intense neutron source at the Paul Scherrer Institut (PSI) in Switzerland [58].

It is anticipated that the coating technology can be improved, leading to a factor of 3 improvement in the figure of merit, equation (34). It is also anticipated that the storage lifetime could be improved to perhaps 200 s. However, the principal advantage is to increase the UCN density by use of a solid deuterium spallation-driven ultracold neutron source.

The idea that solid deuterium can be used as a UCN source is due to Golub and Böning who first discussed its use in the context of a thin film source [59]. Pokotilovskii suggested a configuration that would work at a pulsed neutron source, with the UCN being produced during the short duration of an intense neutron pulse and conducted to a UCN storage vessel, and then isolated from the UCN storage vessel by a fast valve so that the produced UCN would not be lost in the deuterium which has a relatively high loss cross-section [60]. The advantages of enclosing a neutron spallation target and solid deuterium in a flux trap are discussed in [61], and this discussion led to the construction of a prototype source at Los Alamos National Laboratory (LANL) that produced 140 UCN cm^{-3} in a storage vessel above the source [62]. This is to be compared to the output of the ILL UCN source which, in a similar storage volume, produced about 40 UCN cm^{-3}.

For the PSI source, it is planned to use 30 l of solid deuterium, compared to 1 l or less for the LANL source. Comparisons between the configurations are difficult as the LANL source uses cold polyethylene as the flux trap and spallation neutron moderator, while the PSI source uses heavy water as the moderator, with the solid deuterium apparently serving as the UCN

converter and the cold moderator. One might expect a larger density from the polyethylene moderator for the moderation length is about 2 cm in hydrogenous materials, compared to 25 cm in heavy water. However, the absorption rate is relatively low, with a neutron lifetime of about 0.2 s in heavy water compared to 0.16 ms in polyethylene. So the moderated neutrons occupy a 1000 times larger volume in the heavy water system, with a lifetime 1000 times longer, and are limited by the diffusion time out of the heavy water central region. With all these factors canceling overall in the comparison, the principal means of increased density of the PSI source is the increase of the current in the spallation source, 2 mA compared to 100 μA in the LANL prototype source. Simply scaling by the currents suggests a density of about 3000 UCN cm^{-3} for the PSI source, comparable to their own estimates.

In evaluating the experimental sensitivity, it is assumed that the EDM experiment can be filled with UCN with 50% efficiency. This is ambitious in that the ILL experiment, given a source density of 40 cm^{-3}, produces a net UCN density of 5 cm^{-3} for the 1990 experiment, which is due in part that only the neutrons surviving after the storage period contribute to the measurement. Applying these factors to the Hg comagnetometer experiment, along with an anticipated increase in storage time to 200 s, and an increase in the electric field to 15 kV cm^{-1}, shows an increase in the figure of merit, equation (34), compared to the present comagnetometer experiment (which produced a limit of 3×10^{-26} e cm) by a factor of 100; therefore, a limit of 3×10^{-28} e cm appears imminently feasible.

However, attaining this level of accuracy will require very careful control of the geometric phase effect. The magnetic shields presently in use do not have an adequate small gradient to eliminate this effect. The plan is to install a number of discrete alkali atom magnetometers that will allow control of the field gradients in real time. Other comagnetometer issues that were discussed earlier also need to be addressed.

It is anticipated that the refurbished apparatus will be taking data in the late 2010s.

7.2. PNPI experiment at ILL

A multicell experiment being built under the direction of A P Serebrov is nearing completion at the ILL [63].

This ambitious project employs 13–20 l storage volumes, with an anticipated voltage of 15 kV cm^{-1}. The systematic magnetic fields will also be monitored with 16 discrete magnetometers. The experiment will be operated in exactly the same fashion as the earlier ILL and PNPI experiments. In some sense, the experiment is equivalent to running 13 copies of the earlier experiments together, although having the storage bottles in the same apparatus allows detection and cancellation of common mode magnetic field fluctuations. The storage cells will be oriented with their long dimension vertical, so the offset in the center of mass from the geometrical mean might be problematic. The general magnetometer problem remains, as described in section 5.2. With present operating conditions of this experiment, a limit three times better than the current limit can be obtained in three years of running.

8. The future: superfluid ^{4}He

8.1. The production of UCN in superfluid ^{4}He

To increase the sensitivity of UCN EDM experimental searches, an increase in UCN density is required. Both planned and existing UCN sources, based on extraction of UCN from a cold moderator, are limited by the phase-space density of low-energy neutrons in the moderator. At most, one could expect a factor of perhaps 10 over the density at the ILL reactor, but this requires the extension of reactor technology by about an order of magnitude in regard to

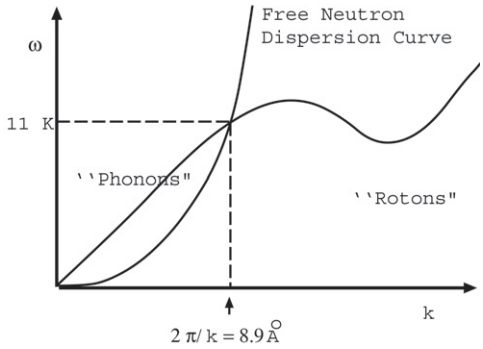

Figure 8. Free neutron and superfluid ^{4}He elementary dispersion curves.

radiation fluxes in the core. Spallation sources might eventually give a factor of 100 increase in density, but this remains to be proven.

There is another way to produce UCN; the idea is to inelastically scatter cold neutrons in a suitable material. As the neutron wavelength increases, the inelastic scattering efficiency of solids and liquids decreases. Thus, the rate of scattering from high to low energy can exceed the inverse, that is, scattering from low to high energy. In a suitable material, the density of low-energy neutrons can be enhanced over what is expected from the source phase-space density.

An ideal material for such a UCN source is superfluid ^{4}He [64]. ^{4}He has zero neutron absorption because it is the most tightly bound nucleus. Thus, if the superfluid bath is sufficiently free of ^{3}He (which has a rather large absorption cross-section), UCN can be stored in the bath until β decay, wall absorption or upscattering occurs; it is expected that with modest effort, β decay can become the dominant loss mechanism.

The production of UCN by the downscattering of 8.9 Å neutrons in superfluid He has now been demonstrated and well studied [65, 66]. The process is nicely described in [9]. Figure 8 shows the free neutron dispersion curve along with the dispersion curve for elementary excitations in superfluid ^{4}He (the Landau–Feynman (LF) dispersion curve). The dispersion relation of the free neutron, relating the energy to the momentum, is a parabola:

$$\omega = \hbar k^2/2m. \tag{57}$$

This curve crosses the L-F dispersion curve at $2\pi/k^* = 8.9$ Å and $E^* = \hbar\omega = 11$ K. The crossing point is in the quasi-linear region of the LF curve. (The curves also intersect at $k = 0$.) Neutrons in this range of wavelength are readily produced by a liquid deuterium or liquid hydrogen moderator.

Because both energy and momentum are conserved in the scattering process, neutrons at or near rest can only absorb phonons of energy E^*, where the dispersion curves cross. This process is strongly suppressed by the Boltzmann factor, $e^{-E^*/T}$, when the superfluid temperature is less than 1 K. By the same argument, only neutrons with energy near E^* can scatter into the UCN energy region by emission of a single excitation.

A UCN source based on this process operates by the following principle. Neutrons of wavelength 8.9 Å can easily penetrate the walls of the storage container and enter the superfluid bath. These neutrons then downscatter, producing UCN which are trapped in the container. (U_F for liquid ^{4}He is about 20 neV, much less than the potential for most solid materials, so we can assume that it is zero in the following discussion.) UCN produced in this way will remain in the superfluid He bath until they are lost through one of the possible loss mechanisms, which

include β decay, absorption by ^{3}He and loss in the wall. The UCN will reach a saturation density

$$\rho_{\rm UCN} = P\tau, \tag{58}$$

where τ is the total loss rate,

$$\tau^{-1} = \tau_{\rm wall}^{-1} + \tau_{\beta}^{-1} + \tau_{^3{\rm He}}^{-1} + \cdots \tag{59}$$

and P is the UCN production rate (UCN/(cm^3 s)) due to the above-mentioned downscattering process [67],

$$P = 7.2\frac{{\rm d}^2\Phi^*}{{\rm d}\lambda\,{\rm d}\Omega}\frac{1}{\lambda_{\rm u}^3}\delta\Omega\ {\rm UCN\ cm^{-3}\ s^{-1}}, \tag{60}$$

where the neutron spectral density is specified at 8.9 Å, $\lambda_{\rm u}$ is the shortest UCN wavelength that can be stored in the container and $\delta\Omega$ is the source solid angle subtended at the superfluid bath. A UCN source based on this principle is referred to as a 'superthermal source'. When a broad spectrum neutron beam is used, multiphonon processes increase the production rate by about 30% [68].

The neutron–superfluid ^{4}He system is in some sense a two-level quantum system, and the production of UCN by the emission of a phonon can be compared to the spontaneous emission of radiation by an excited atom.

Cold neutrons of wavelength 8.9 Å have an attenuation length of order 100 m in superfluid ^{4}He at temperatures at around 1 K. Thus, for any conceivable experiment, the production rate will be constant (except for beam divergence) independent of position along the incident neutron beam.

The increase in neutron density near zero energy can be understood by the following argument. If we take a linear dispersion relation for the liquid He elementary excitations, $\omega = ck$ where c is the phonon (sound) velocity, we have the following condition, by conservation of energy and momentum, limiting the region around $k = k^* + \delta k$ which can scatter to an UCN with momentum $k_{\rm UCN}$:

$$c|\vec{k} + \vec{k}_{\rm UCN}| = \frac{\hbar}{2m}\left(k^2 - k_{\rm UCN}^2\right). \tag{61}$$

The maximum and minimum of $|\vec{k} + \vec{k}_{\rm UCN}|$ are $k \pm k_{\rm UCN}$. We thus arrive at

$$\delta k = 2k_{\rm UCN}. \tag{62}$$

This is a remarkable result and shows that Liouville's theorem, which was previously briefly mentioned, is apparently violated by this system. Incident neutrons occupy a (momentum) phase-space volume of $4\pi k^{*2}\delta k$ whereas the UCN occupy a volume $\frac{4\pi}{3}\,k_{\rm UCN}^3$, which represents a factor of $\frac{1}{3}(k_{\rm UCN}/k^*)^2$ decrease in the phase-space volume, corresponding to an increase in the phase-space density. Given an arbitrarily long storage lifetime of the UCN, for any non-zero production rate P, the real space density will simply continue to increase as the incident neutrons downscatter, at least until the UCN density is so high that all the states of the Fermi gas are occupied, at which point no more downscattering can occur. This is possible because the produced phonons occupy a very large phase space, and these phonons are continually removed from the system by a refrigerator which keeps the superfluid bath cold. In this regard, the system is analogous to a heat-powered refrigerator. Of course UCN losses limit the ultimate density achieved, equation (58).

We have not addressed upscattering of UCN by phonons which leads to additional losses. The one phonon process is easy to calculate. By using microscopic reversibility [18] the

production and upscattering processes can be related,

$$\frac{\sigma(E^* \to E_{\rm UCN})}{E_{\rm UCN}\, {\rm e}^{-E_{\rm UCN}/T}} = \frac{\sigma(E_{\rm UCN} \to E^*)}{E^*\, {\rm e}^{-E^*/T}}, \tag{63}$$

which implies that the reverse process is exponentially small, as was previously mentioned. However, this simple treatment does not include higher order processes, and in fact the dominant process below 1K is two-phonon upscattering [69], which gives a loss time of about $\tau = 100T^{-7}$ s.

If the incident neutrons are polarized, the UCN that are produced will also be polarized because there are no magnetic process in the scattering interaction. This suggests that in experiments where polarized UCN are required, a considerable improvement can be gained by using a polarized cold beam which can be polarized to a very high level with negligible loss.

8.2. SNS superfluid helium experiment

The possibility of a new neutron EDM experiment employing spin polarized ^{3}He stored together with UCN in a superfluid bath was first described in detail in [70]. Detailed reports describing the current status of efforts to implement this system are available in [71]. Here, we will give an overview of the advantages of this experimental technique and describe some of the special features of the system that tend to get buried in detailed reports.

Attempts to make a UCN source based on the superthermal process in ^{4}He all encountered technical difficulties, primarily in regard to extraction of the UCN from the bath. Invariably and inevitably, the thin material windows used to contain the liquid He but allow the UCN to pass, become covered by condensed, frozen gases (O_2 or N_2), increasing $U_{\rm F}$ and/or the UCN absorption. Typically, extracted densities have been a factor of 10–100 below that expected [66, 72]. Indirect measurement through the upscattering rate has confirmed that the expected density does indeed exist within the bath [73]. Recently, workers at Munich have constructed a helium source without a UCN exit window that shows the expected UCN density [74].

The extraction problems can be avoided by performing an EDM search directly in the liquid helium of the superthermal source. Such a system has a number of advantages; for example, because of the excellent dielectric properties of liquid helium, increasing the applied electric field by nearly an order of magnitude might be possible.

We can estimate the figure of merit, equation (34), of a superfluid helium experiment operated at the Spallation Neutron Source (SNS) presently under construction at Oak Ridge National Laboratory. It has been anticipated that a polarized UCN production rate of up to 5 cm^{-3} s^{-1} is possible at the SNS, which with a storage lifetime of 500 s implies a UCN density of 2500 cm^{-3} in the experimental apparatus. Application of an electric field of 50 kV cm^{-1} appears possible, and comparing with the ILL Hg comagnetometer experiment (which has produced the present best experimental upper limit), we see an increase in the figure of merit by a factor of 1200, indicating that a level of sensitivity approaching 2×10^{-29} e cm appears feasible.

The important point is that the UCN are produced in the experiment in the polarized state, so the usual losses associated with transport from a source to the experiment, and with polarization, are eliminated. The other advantage is that the electric field can be significantly increased, and at low temperatures enhanced storage times can be expected.

It is interesting to note that the figure of merit, equation (34), is linear in the storage time T (taken as equal to the coherence time) because the UCN density is proportional to T.

Also, it appears feasible to use a dilute solution of polarized ^{3}He as a UCN spin analyzer, detector and magnetometer. ^{3}He only absorbs neutrons when the total spin is zero because the reaction occurs via the 0^+ excited state [75] as follows:

$$^3\mathrm{He} + \mathrm{n} \rightarrow \mathrm{p} + \mathrm{T} + 764\ \mathrm{keV}. \tag{64}$$

The polarization and cryogenic transport of polarized ^{3}He have also been studied [76]. Furthermore, energetic charged particles produce ultraviolet scintillations in liquid helium with about four photons per keV of the deposited energy. The reactions between ^{3}He and neutrons in the liquid helium are thus easily detected, giving a detection of reactions with nearly 100% efficiency. See [77] for an application of these techniques to a measurement of the neutron β decay lifetime which may lead to a factor of 100 improvement in accuracy.

The ^{3}He serves as a UCN polarizer by absorbing neutrons in the singlet state. To be effective, this rate of absorption should be slightly higher than other UCN loss mechanisms in the system. This implies a ^{3}He concentration of 10^{-10}, or about 10^{12} atoms/cm^3. Such low densities of polarized ^{3}He can be produced with a hexapole state selector, with essentially perfect polarization, which has been demonstrated at Los Alamos. Other techniques for producing higher densities have polarization limited to 70%; since the ^{3}He serves three functions, it is expected that the experimental sensitivity varies as at least the square of the ^{3}He polarization. This agrees with detailed calculations.

An EDM experiment based on these ideas, as originally proposed, could be sensitive to a neutron EDM by looking at the scintillation rate at the end of a double-pulse sequence, as a function of electric field polarity [78]. It has been shown by solving the Schrödinger equation with a spin-dependent absorption probability that this technique is slightly less sensitive that the conventional bottle technique; however, this loss of sensitivity is more than made up for by elimination of the extraction losses and increase in the electric field.

In the following discussion, let the subscript 3 refer to the ^{3}He atoms, and subscript n refer to the UCN. In the case where both species are polarized, the spin-dependent loss rate can be written as

$$\frac{1}{\tau_{\mathrm{abs}}} = \frac{1}{\tau_{^3\mathrm{He}}}(1 - \vec{p}_{\mathrm{n}} \cdot \vec{p}_3) = (1 - p_{\mathrm{n}} p_3 \cos\theta_{\mathrm{n3}})/\tau_{^3\mathrm{He}}, \tag{65}$$

where θ_{n3} is the angle between the spin polarization vectors and $|\vec{p}_{\mathrm{n},3}| \leqslant 1$. Each loss (nuclear reaction) produces a scintillation pulse; the scintillation rate thus becomes a measure of the angle between the polarization vectors.

One could search for a neutron EDM by using the above UCN production/polarization technique. After the UCN are polarized (along a static field of magnitude B_0), the UCN and ^{3}He spins could be flipped by $\pi/2$; the spins then precess about the static field and there will be a modulation in the scintillation rate:

$$\phi(t) \propto (1 - \vec{p}_3 \cdot \vec{p}_{\mathrm{n}}) = 1 - p_3 p_{\mathrm{n}} \cos[(\gamma_3 - \gamma_{\mathrm{n}}) B_0 t + \Phi], \tag{66}$$

where $\phi(t)$ is the time-dependent scintillation rate, Φ is an arbitrary phase, and, for the analysis presented in this section, the gyromagnetic ratios are taken with angular frequency units,

$$\gamma_{\mathrm{n}}/2\pi \approx -3\ \mathrm{Hz/mG}$$

and

$$\gamma_3/2\pi \approx -3.33\ \mathrm{Hz/mG}.$$

The EDM of ^{3}He is expected to be quite small (due to shielding as described in section 6.1); thus, if an electric field is applied along B_0 there will be a change in the frequency of the scintillation rate modulation. Unfortunately, the problem of measuring the

magnetic field remains (although the effects are only 1/10 as large since the gyromagnetic ratios are nearly equal) and it has been demonstrated that experiments are presently limited by magnetic systematic effects. It might be possible to use SQUID magnetometers to detect the precessing ^{3}He magnetization, so that the ^{3}He could then serve as a direct magnetometer. Recent advances in SQUID technology make this a possible alternative to the dressed spin technique described below.

8.2.1. Dressed spin magnetometry. In the above description, it is evident that a perfect experiment would be possible if the magnetic moments of the ^{3}He and neutron were equal; the fact that the magnetic moments are equal to within 10% reduces the sensitivity to background field by an order of magnitude, and if the moments were exactly equal, there would be no effect at all. Unfortunately, we have no direct control over the physics responsible for the observed magnetic moments; however, these moments can be artificially modified by using 'dressed atom' techniques [79], and it is possible to make them equal [70].

In the presence of a strong oscillating magnetic field, the magnetic moment will be modified, or 'dressed', yielding an effective gyromagnetic ratio, in the limit $\gamma B_0 \ll \omega_{\rm RF}$

$$\gamma' = \gamma J_0(\gamma B_{\rm RF}/\omega_{\rm RF}) = \gamma J_0(x), \tag{67}$$

where γ is the unperturbed gyromagnetic ratio, $B_{\rm RF}$ and $\omega_{\rm RF}$ are the amplitude and frequency of an applied oscillating magnetic RF field, and J_0 is the zeroth-order Bessel function. This effect can be qualitatively understood by taking the average of the spin in an oscillating magnetic field. Consider a spin pointing along $\hat{z}$ at $t = 0$. Now apply an oscillating field along $\hat{x}$; the spin precession frequency is time dependent,

$$\omega(t) = \dot{\theta}(t) = \gamma B_x(t) = \gamma B_{\rm RF} \sin \omega_{\rm RF} t,$$

so that the angle relative to $\hat{z}$ is

$$\theta = \gamma (B_{\rm RF}/\omega_{\rm RF}) \cos \omega_{\rm RF} t.$$

The average spin projection $\langle P_z \rangle$ along $\hat{z}$ is given by

$$\langle P_z \rangle = \frac{1}{T} \int_0^T \cos \left[\frac{\gamma B_{\rm RF}}{\omega_{\rm RF}} \cos \omega_{\rm RF} t \right] {\rm d}t = J_0(\gamma B_{\rm RF}/\omega_{\rm RF}) = J_0(x).$$

A more sophisticated treatment shows that a spin will respond to a small (compared to the oscillating field amplitude) static field along $\hat{x}$, with an average magnetic moment $\gamma' = \gamma J_0(x)$; our simple estimate gives a picture of how the oscillating field dilutes the magnetic moment.

In practice, the oscillating field is at right angles to the static field B_0 around which the spins are precessing. In the absence of the oscillating field, one would see scintillation due to reactions occurring at a rate given by (66). Thus, there is an oscillation in the scintillation rate at the difference in the precession frequencies [$\delta\omega = (\gamma_{\rm n} - \gamma_3) B_0$]. If the RF dressing field is now applied, the effective magnetic moments become modified, and, defining x in terms of $\gamma_{\rm n}$

$$\delta\omega = [\gamma_{\rm n} J_0(x) - \gamma_3 J_0(\gamma_3 x/\gamma_{\rm n})] B_0. \tag{68}$$

This has the property that $\delta\omega = 0$ when $x \approx 1.19 \equiv x_c$; this condition is referred to as 'critical dressing'. It can be achieved in practice with a dressing field frequency of order 1 kHz and an amplitude of 100 mG, and a spin precession frequency on the order of a few hertz.

If the neutron EDM is non-zero, the neutron precession frequency will be shifted by an amount $2 d_{\rm n} E J_0(\gamma_{\rm n} x)$ (since the dressing dilutes the net spin projection). Thus, the value of $x = x_{\rm c}$ to give $\delta\omega = 0$ is changed. By measuring the value of $x_{\rm c}$ versus electric field direction, a neutron EDM would be evident. The important point is that the effect of static magnetic fields is cancelled.

Experimentally, the neutron and helium spin vectors could be kept nearly parallel; the scintillation would increase or decrease as x is varied away from the value x_c such that $\delta\omega = 0$. Over the course of a storage period, x could be sinusoidally modulated at a low frequency ω_m and the value $x_c(\pm E)$ inferred from variations in the scintillation rate which occur at harmonics of ω_m. If the average value of $x \neq x_c$, there will be a first harmonic to the scintillation rate growing linearly in time. If $x = x_c$, there will be only a second harmonic component. In practice, a feedback system might be used to force the first harmonic signal to zero; the second harmonic then serves as a system calibration. (Note that the modulation in x and the subsequent modulation in the scintillation rate are 90° out of phase because the spin vectors must precess before the effects due to a change in x are manifest.)

A detailed analysis of this system is given in [70], in which many technical issues are addressed. It is shown that a factor of over 1000 improvement in the neutron EDM experimental limit is feasible. This improvement is based on a factor of 5 increase in electric field strength, an increase in the net UCN storage lifetime and an increase by a factor of nearly 10^4 in UCN density. Magnetic field noise and systematic effects are eliminated by the dressed spin technique.

An important difference between the previous UCN storage experiments and one performed directly in the superfluid bath is that essentially all of the UCN stored in the liquid helium contribute to the measurement. As was shown earlier, the ILL experiment UCN-use efficiency was only 3%, giving an effective experimental density of 4 cm^{-3}. This number should be compared to the 2×10^5 cm^{-3} given above for the superthermal source.

8.2.2. Analysis of the dressed spin system and systematic effects. The motion of a spin under the application of static and non-resonant oscillating magnetic fields is quite complicated. In some sense, saying that the magnetic moment is modified (or dressed) is the 'zeroth-order' approximation. In [70], the system was studied both by numerically integrating the equations of motion and through quantum perturbation theory. The ^{3}He–n spin system was solved numerically under various conditions. This system is difficult to solve numerically since it involves two time scales: the RF field of 1 kHz and the relatively slow precession (1 Hz) around the dc field. The accuracy obtained is set by the step size at the 1 kHz level. The results were identical to those obtained with the analytical treatment.

Briefly, in the quantum treatment, effects of static fields both along the RF field (B_0^x, which is a spurious field) and perpendicular to the RF field (applied field $B_0^z \gg B_0^x$) were studied. The unperturbed states are specified by $|\pm 1/2\rangle|n\rangle$, where n is the RF field photon number. The states are degenerate between $\pm 1/2$ before the static fields are applied. Using the formalism developed in [79], the following first-order correction (due to B_0^z) to the $\pm 1/2$ eigenvalues was found:

$$E^{(1)} = \pm\tfrac{1}{2}\gamma\sqrt{\left(B_0^x\right)^2 + \left[B_0^z J_0(\omega_1/\omega_{RF})\right]^2}, \tag{69}$$

where $\omega_1 = \gamma B_{RF}$. If we require that $E_3^{(1)} = E_n^{(1)}$, the critical dressing condition is obtained. Thus, effects of $B_0^x \neq 0$ enter only in second order. Carrying the perturbation expansion to higher order mixes in states of different n. The second-order corrections are zero, while the third order gives $E^{(3)} \propto \left(\gamma B_0^z\right)^3/\omega_{RF}^2$, which shows that fluctuations in the precession field $\delta\omega_0$ only alter the critical dressing condition to order

$$\delta x_c = (\omega_0/\omega_{RF})^2(\delta\omega_0/\omega_0). \tag{70}$$

With $\omega_0/\omega_{RF} \approx 10^{-2}$, the system shows excellent rejection of static field fluctuations.

An important result of this analysis is that the spin/field state cannot be affected by the static electric field in the absence of an edm. The total system angular momentum could be

greater than or equal to 1; however, there is no way for the static electric field to couple to the constituent system states (RF photons or particles of spin-1/2).

8.3. CryoEDM at ILL

An experiment presently under construction at the ILL is described in the proposal [80]. This experiment will be conducted in nearly the same way as the 1990 ILL experiment, except that the apparatus will be filled with superfluid helium. The UCN will be produced by the superthermal process in a region away from the storage cell, and then conducted into the storage cell, with EDM measurements performed as in the 1990 experiment. The Rb magnetometers will be replaced with SQUID magnetometers that will be placed in the region around the storage cell. The problems associated with external discrete magnetometers remain, but the leakage currents associated with the application of high voltage should be orders of magnitude less than the room temperature experiment, which should decrease the potential systematic. The figure of merit, equation (34), compared to the ILL Hg comagnetometer (current best limit) result is about a factor of 20 greater, therefore it is anticipated that a level of 10^{-27} e cm can be obtained.

A novel UCN detector has been developed for this experiment that allows detection directly in a superfluid filled guide. The detectors employ ^{6}Li deposited directly on a large area PN photodiode detector. The detector can be further coated with a magnetic thin film polarizer, which will make for a complete polarization analysis system for the UCN.

9. Conclusions

The fundamental nature of *CP* non-invariance in high-energy interactions remains largely unknown. The search for the neutron EDM remains among the most sensitive ways to test theoretical notions regarding the nature of the interactions that led to, for example, the matter–antimatter asymmetry of the universe.

The current experimental limit is based on a UCN storage experiment that employs a ^{199}Hg atomic spin precession magnetometer. In this work, a new 'geometric phase' systematic was discovered that results from an interference between the motional $\vec{E} \times \vec{v}$ magnetic field and a magnetic gradient. This effect was accounted for, and appears as controllable in improved experiments.

Current plans for improving the neutron EDM experimental limit include moving the Hg comagnetometer experiment to a new intense UCN source based on solid deuterium now under construction at PSI. With upgrades to the experiment, including reduction of gradients that lead to the geometric phase systematic, and increase in the electric field and UCN storage lifetime, it is anticipated that an EDM limit in the 10^{-27} e cm range, or better, will be possible. This experiment will likely produce the first improved neutron EDM limit among the new experiments discussed in this paper.

Other experiments that do not employ a comagnetometer are being developed, or are under construction. Given the past problems with discrete external magnetometry in accounting for systematic magnetic fields, a non-zero result from any of these experiments should be considered with skepticism. In fact, a zero result should be considered with similar skepticism, for we are now in a range of sensitivity where both zero and non-zero results have far-reaching theoretical implications. It should also be noted that the presence of the Hg comagnetometer in the most recent ILL EDM result was crucial for understanding the geometric phase systematic.

The superfluid helium EDM experiment planned for the SNS is the only experiment presently under discussion that has potential to attain a sensitivity in the 10^{-28} e cm range. This experiment is very ambitious and will most likely not be producing data until after 2012.

Note added in proof. Figures 1, 2, 3, 4, 6, 7 and 8 are in the public domain. Source: S K Lamoreaux.

References

[1] Kellog J M B, Rabi I I, Zacharias J R and Ramsey N F 1940 *Phys. Rev.* **57** 677
Kellog J M B, Rabi I I, Zacharias J R and Ramsey N F 1939 *Phys. Rev.* **55** 318
[2] Purcell E M and Ramsey N F 1950 *Phys. Rev.* **78** 807
[3] Smith J H, Purcell E M and Ramsey N F 1957 *Phys. Rev.* **108** 120
[4] Lee T D and Yang and C N 1956 *Phys. Rev.* **104** 254
[5] Wu C S *et al* 1960 *Phys. Rev. Lett.* **5** 430
[6] Ramsey N F 1958 *Phys. Rev.* **109** 225
[7] Griffith W C, Swallows M D, Loftus T H, Romalis M V, Heckel B R and Fortson E N 2009 *Phys. Rev. Lett.* **102** 101601
[8] Khriplovich I B and Lamoreaux S K 1997 *CP Violation Without Strangeness* (Berlin: Springer)
[9] Golub R, Richardson D J and Lamoreaux S K 1991 *Ultracold Neutrons* (Bristol: Hilger)
[10] Chadwick J and Goldhaber M 1934 *Nature* **134** 237
Chadwick J and Goldhaber M 1935 *Proc. R. Soc.* A **151** 479
[11] Snell A H and Miller L C 1948 *Phys. Rev.* **74** 1217
[12] Fermi E 1935 *Phys. Rev.* **48** 570
[13] Amsler C *et al* 2008 (Particle Data Group) *Phys. Lett.* B **667** 1
[14] Fermi E and Marshall L 1947 *Phys. Rev.* **71** 666
[15] Peshkin and Ringo 1971 *Am. J. Phys.* **39** 324
[16] Landau L D and Lifshitz E M *Quantum Mechanics* 2nd edn (Oxford: Pergamon)
[17] Sears V F 1989 *Neutron Optics* (London: Oxford University Press)
[18] Turchin V F 1965 *Cold Neutrons* (Program for Scientific Translations, Israel)
[19] Foldy L L 1945 *Phys. Rev.* **67** 107
[20] Ramsey N F 1956 *Molecular Beams* (London: Oxford University Press)
[21] Fermi E 1962 *Collected Papers* (Chicago, IL: University of Chicago Press) pp 639–41
[22] Maier-Leibnitz H and Springer T 1963 *J. Nucl. Energy A/B* **17** 217
[23] Zeldovich Ya B 1959 *Sov. Phys.—JETP* **9** 1389
[24] Lamoreaux S K and Golub R 1994 *Phys. Rev.* D **50** 5632
[25] Sandars P G H and Lipworth E 1964 *Phys. Rev. Lett.* **13** 718
[26] Pendelbury J M 1988 *Proc. 9th Symp. on Grand Unification* (France, Aix-Les Bains)
[27] Altarev I S *et al* 1986 *Sov. Phys.—JETP Lett.* **44** 460
[28] Smith K F *et al* 1990 *Phys. Lett.* B **234** 33
[29] Altarev I S *et al* 1996 *Phys. At. Nucl.* **59** 1152
[30] Harris P G *et al* 1999 *Phys. Rev. Lett.* **82** 904
[31] Lamoreaux S K and Golub R 2000 *Phys. Rev.* D **61** 051301
[32] Harris P G *et al* 1999 *Phys. Rev. Lett.* **82** 904
[33] Ramsey N F 1984 *Acta Phys. Hung.* **55** 117
[34] Brian Hyslop W and Lauterbur P C 1991 *J. Mag. Res.* **94** 501
[35] Schmid R, Plaster B and Filippone B W 2008 *Phys. Ref.* **78** 023401
[36] Jacobs J P *et al* 1995 *Phys. Rev.* A **52** 3521
[37] Vold T G *et al* 1984 *Phys. Rev. Lett.* **52** 2229
[38] Commins E D, Ross S B, DeMille D and Regan B C 1994 *Phys. Rev.* A **50** 2960
[39] Lamoreaux S K 1996 *Phys. Rev.* A **53** R3705
[40] Abragam A 1962 *Principles of Nuclear Magnetism* (London: Oxford University Press)
[41] Happer W 1970 *Phys. Rev.* B **1** 2203
[42] Ramsey N F 1988 private communication
[43] Commins E D 1991 *Am. J. Phys.* **59** 1077
[44] Hunter L R 2004 private Communication
[45] Pendlebury J M *et al* 2004 *Phys. Rev.* A **70** 032102
[46] Berry M 1984 *Proc. R. Soc. Lond.* A **392** 45

[47] Ramsey N F 1955 *Phys. Rev.* **100** 1191
[48] Baker C A *et al* 2006 *Phys. Rev. Lett.* **97** 131801
[49] Lamoreaux S K and Golub R 2005 *Phys. Rev.* A **71** 032104
[50] Barabanov A L, Golub R and Lamoreaux S K 2006 *Phys. Rev.* A **74** 02115
[51] Golub R and Swank C 2008 arXiv:0810.5378
[52] Lamoreaux S K and Golub R 2007 *Phys. Rev. Lett.* **98** 149101
[53] Baker C A *et al* 2007 *Phys. Rev. Lett.* **98** 149102
[54] Harris P G and Pendlebury J M 2006 *Phys. Rev.* A **73** 014101
[55] Lamoreaux S K 1989 *Nucl. Instrum. Methods* A **284** 43
[56] Pendlebury J M 1992 *Nucl. Phys.* A **546** 359c
[57] Jacobs J P, Klipstein W M, Lamoreaux S K, Heckel B R and Fortson E N 1995 *Phys. Rev.* A **52** 3521
Jacobs J P, Klipstein W M, Lamoreaux S K, Heckel B R and Fortson E N 1993 *Phys. Rev. Lett.* **71** 3782
[58] Kirch K 2006 Cape Code Lepton Moments Meeting http://nedm.web.psi.ch/
[59] Golub R and Böning K 1983 *Z. Phys.* B **51** 95
[60] Pokotilovskii Y N 1995 *Nucl. Instrum. Methods* A **356** 412
[61] Lamoreaux S K 2001 arXiv:nucl-ex/0103005
[62] Saunders A *et al* 2004 *Phys. Lett.* B **595** 55
[63] Serebrov A P 2004 *Int. Conf. Prec. Meas.* with slow neutrons, NIST, Gaithersburg, 5–7 April; see also, http://cns.pnpi.spb.ru/ucn/articles/Serebrov1.pdf
[64] Golub R and Pendlebury J M 1977 *Phys. Lett.* A **62** 3376
[65] Ageron P *et al* 1978 *Phys. Lett.* A **66** 469
[66] Golub R *et al* 1983 *Z. Phys.* B **51** 187
[67] Lamoreaux S K and Golub R 1995 *Pis'ma ZhETF* **58** 844
Lamoreaux S K and Golub R 1993 *Sov. Phys. JETP Lett.* **58** 792
[68] Korobkina E *et al* 2002 *Phys. Lett.* A **301** 462
[69] Golub R 1979 *Phys. Lett.* A **72** 387
[70] Golub R and Lamoreaux S K 1994 *Phys. Rep.* **237** 1
[71] http://p25ext.lanl.gov/edm/edm.html
[72] Yoshiki H *et al* 1992 *Phys. Rev. Lett.* **68** 1323
Golub R and Lamoreaux S K 1993 *Phys. Rev. Lett.* **70** 517
[73] Kilvington A I *et al* 1987 *Phys. Lett.* A **125** 416
[74] Zimmer O *et al* 2007 *Phys. Rev. Lett.* **99** 104801
[75] Passell L and Schermer R 1960 *Phys. Rev.* **150** 146
[76] Aminoff C G *et al* 1989 *Rev. Phys. Appl.* **24** 827
[77] Doyle J M and Lamoreaux S K 1994 *Europhys. Lett.* **26** 253
Huffman P R *et al* 2000 *Nature* **403** 64
[78] Golub R 1983 *J. Physique* **44** L321
Golub R 1987 *Proc. 18th Int. Conf. on Low-Temperature Physics, Part 3; Invited Papers* (Kyoto) p 2073
[79] Polonsky N and Cohen-Tannoudji C 1965 *J. Physique* **26** 409
Cohen-Tannoudji C and Haroche S 1969 *J. Physique* **30** 153
[80] Balashov S N *et al* 2007 arXiv:0709.2428